AD NUMBER

AD270501

LIMITATION CHANGES

TO:

Approved for public release; distribution is unlimited.

FROM:

**Distribution authorized to U.S. Gov't. agencies and their contractors;
Administrative/Operational Use; JAN 1962. Other requests shall be referred to Air Force Engineering Development Center, Arnold AFB, TN.**

AUTHORITY

usaedc ltr 17 sep 1975

AEDC-TDR-62-9

AN INVESTIGATION OF BASE HEATING ON A 5.47-PERCENT-SCALE MODEL SATURN SA-1 BOOSTER AFTERBODY AT MACH NUMBERS 1.63 AND 3.07

By

John G. Dawson, Jr.
Rocket Test Facility
ARO, Inc.

TECHNICAL DOCUMENTARY NO. AEDC-TDR-62-9

January 1962

AFSC Program Area 921E, Project 9018

(Prepared under Contract No. AF 40(600)-800 S/A 24(61-73) by ARO, Inc., contract operator of AEDC, Arnold Air Force Station, Tenn.)

ARNOLD ENGINEERING DEVELOPMENT CENTER
AIR FORCE SYSTEMS COMMAND
UNITED STATES AIR FORCE

NOTICES

Qualified requesters may obtain copies of this report from ASTIA. Orders will be expedited if placed through the librarian or other staff member designated to request and receive documents from ASTIA.

When Government drawings, specifications or other data are used for any purpose other than in connection with a definitely related Government procurement operation, the United States Government thereby incurs no responsibility nor any obligation whatsoever; and the fact that the Government may have formulated, furnished, or in any way supplied the said drawings, specifications, or other data, is not to be regarded by implication or otherwise as in any manner licensing the holder or any other person or corporation, or conveying any rights or permission to manufacture, use, or sell any patented invention that may in any way be related thereto.

ASTIA RELEASE TO OTS IS NOT AUTHORIZED

AN INVESTIGATION OF BASE HEATING ON A 5.47-PERCENT-SCALE MODEL SATURN SA-1 BOOSTER AFTERBODY AT MACH NUMBERS 1.63 AND 3.07

By

John G. Dawson, Jr.

Rocket Test Facility

ARO, Inc.

a subsidiary of Sverdrup and Parcel, Inc.

January 1962

ARO Project No. 114108

ABSTRACT

An investigation was conducted to determine the base recirculation characteristics of several different turbine exhaust ducts on a 5.47-percent-scale model of the Saturn SA-1 Booster afterbody. Hydrogen gas was used to simulate the combustible products of the turbine exhaust. Base heating and base pressure data were taken with external airflow at Mach numbers 1.63 (33,000 to 45,000-ft altitude) and 3.07 (70,000 to 80,000-ft altitude). The effect on base heating and base pressure of one inboard engine inoperative and of altitude variation was also investigated.

The data indicated no base burning resulting from circulation of the combustible turbine exhaust gases. The only base heating observed was that attributed to the recirculation of the rocket engine exhaust products. Base pressures indicated a slight rise at the time of hydrogen initiation. Flame shield calorimeter data indicated the maximum heat transfer rate at the center of the shield to be 113 Btu/ft^2-sec. Flame shield pressure data indicated that the flow out from the flame shield region between adjacent engines became sonic at approximately 60,000-ft altitude.

CONTENTS

TABLES

ILLUSTRATIONS

NOMENCLATURE

A	Area, ft^2
C_p	Pressure coefficient
c_p	Specific heat, Btu/lb-°F
h	Simulated altitude, ft
h_c	Film heat transfer coefficient, Btu/ft^2-sec-°F
M	Mach number
m	Calorimeter slug weight, lb_m
O/F	Ratio of engine oxidizer flow to fuel flow
p	Pressure, psia
$\dot{q}$	Heat transfer rate, Btu/ft^2-sec
q	Dynamic pressure, $lb/in.^2$
T	Temperature, °F
t	Time, sec
γ	Ratio of specific heats

SUBSCRIPTS

B	Base
FS	Flame shield
∞	Free-stream conditions
g	Gas
w	Wall

1.0 INTRODUCTION

The interaction of the external flow stream with the engine exhaust jets and the impingement of the exhaust jets upon each other could produce a flow phenomenon which would result in recirculation of hot, fuel-rich gases into the base of the SA-1 Saturn booster. These gases come from the main engine exhaust and from the propellant pump turbine exhaust, and if combined with atmospheric air, could ignite and burn at the base. Such burning, with the attendant high heat release, may cause damage to vital engine controls and accessories. The phenomenon of base recirculation has been investigated and reported in several technical publications (Refs. 1 and 2). The engine cluster arrangement of the SA-1 Saturn booster presented a base recirculation problem so complex that an estimate of the heat transfer rate to the base could only be obtained by simulated altitude testing. Reference 3 presents results of sub-scale Saturn model testing with subsonic and transonic Mach number external flow conditions.

This report presents the results of a test conducted in the Rocket Test Facility (RTF), Arnold Engineering Development Center (AEDC), Air Force Systems Command (AFSC), with a 5.47-percent-scale model of the Saturn SA-1 Booster afterbody at external flow Mach numbers of 1.63 and 3.07 at altitudes corresponding approximately to expected trajectory altitudes (see Fig. 1 for design trajectory). The purpose of the test was to determine the heat transfer and pressure effects on the missile base caused by (1) the recirculation of engine exhaust gases from the interaction of the rocket exhaust jets with each other and with the external flow stream and (2) the recirculation of the fuel-rich propellant pump turbine exhaust products.

Particular emphasis was placed upon the contribution to base heating and base pressure of several different accessory power turbine exhaust duct configurations. The effects on base recirculation of altitude variation and of one inboard engine inoperative was also noted.

The investigation, conducted during the period July 1 through September 15, 1961, was sponsored by the George C. Marshall Space Flight Center of the National Aeronautics and Space Administration (NASA).

Manuscript released by author January 1962.

2.0 APPARATUS

2.1 TEST ARTICLE

The 5.47-percent-scale model of the Saturn SA-1 Booster afterbody was constructed to match the diameter (13.93 in.) of existing mounting hardware (Figs. 2 and 3). Simulation of the aft shroud contours was provided from model station 0 forward to model station 9.2, which is equivalent to the aft-most 167.5 in. of the prototype booster. That portion of the model forward of model station 9.2 was cylindrical in cross section instead of having the "scalloped" cross section of the prototype booster caused by the eight propellant tanks. Minor external protuberances, such as tie-down lugs, retro-rockets, and umbilical disconnects, were not simulated on the model. Air scoops (Fig. 3) were simulated because it was felt that these would have a direct influence on base heating.

Eight liquid oxygen, RP-1 fueled, rocket engines (Fig. 4), each developing about 500-lb thrust, were used to simulate the prototype engines. A pressurized propellant system was used. Design data on the engines are presented in Table 1. Ignition was accomplished using a pyrophoric fuel, triethylaluminum. The engines were operated at a nominal chamber pressure of 500 psia and at nominal O/F ratio of 2.2.

The model engines were clustered as shown in Fig. 3d with the four inboard engines parallel to the model centerline and the four outboard engines fixed at a 6-deg outboard cant (neutral gimbal position) from the model centerline. This arrangement differed from that of the prototype engine mounting in that the four prototype inboard engines are fixed at a 3-deg outboard cant which could not be duplicated on the model engines because of propellant and coolant line interference forward of the engine mounting plate.

The prototype propellant-pump turbine exhaust gases were simulated by hydrogen gas discharged from "exhausterators" around and for each of the four outboard engines and from overboard ducts for each of the four inboard engines (Fig. 3d). The flow direction (Fig. 5) of the hydrogen gas from the model exhausterator differed from that of the prototype exhausterator because of model hardware interference. Details of model exhausterator design and comparison with the prototype are presented in Fig. 5.

Three overboard duct configurations were investigated; the details of each are shown in Figs. 3 and 6. The long overboard duct configuration was investigated first and most extensively because this was the duct to be used on the first Saturn flights.

2.2 INSTRUMENTATION

Design and fabrication of the model heat shield and flame shield and total heat transfer calorimeters followed closely the concepts proposed in Ref. 4. The shields were of a sandwich-type construction as shown in Figs. 7 and 8. The copper sheet was prepared by sandblasting, followed by plating with cobalt sulfide to produce a black surface of high emissivity. This sheet was backed by 0.38-in.-thick insulation material to reduce heat losses through the back side of the copper. The construction was completed with a solid steel backing plate for structural rigidity.

The calorimeters used to measure total (convective plus radiation) heat transfer were slugs punched from copper sheet prepared in the same manner as the heat shield to give an identical surface. (There were a number of NASA furnished calorimeters installed on the base heat shield but the data from these are not analyzed in this report.) The slugs were inserted into holes cut out of the copper heat shield and were cemented in place with a high-temperature, low-conductivity, ceramic cement in such a way that the slug was flush with the heat shield surface. Twenty-eight gage, chromel-alumel thermocouple wires silver-soldered to the rear face of the slugs were passed through the insulation and backing plate and connected to a temperature recording device. The calorimeter thermocouple millivolt outputs were recorded at 0.6-sec intervals on magnetic tape by a high-speed digital recording system. Playback of this tape on an IBM-7070 computer gave a printed digital output of temperature variation with time.

Heat shield and flame shield pressure measurements were obtained from static pressure orifices mounted flush on the shields. Millivolt outputs from transducers measuring base pressures, plenum chamber total pressure, and test section static pressure were recorded at approximately 1.5-sec intervals and converted to a tabulated digital printout.

Location of all heat shield and flame shield instrumentation is shown in Fig. 7.

Oxidizer and fuel tank pressures, injector pressures, and the individual engine chamber pressures were recorded on continuous direct-inking analog recorders. Individual oxidizer and fuel flows were measured with turbine-type flowmeters, whose frequency outputs were recorded on an oscillograph. Engine coolant system pressures, temperatures, and flows were measured, and safety cut-outs were provided as required to determine and assure proper and safe operation.

One 16-mm movie camera and one television camera were mounted in the test section camera ports (Fig. 9) at the exit plane of the engine

exhaust nozzles to observe and record the ignition sequence and burning pattern of the recirculated combustible gases.

A summary of model and test cell instrumentation showing the method and precision of measuring and recording data is given in Table 2.

2.3 INSTALLATION

The model and centerbody were cantilever-mounted from a spider arrangement in the forward portion of the test cell and extended aft through the nozzle (Fig. 9). The two axisymmetric nozzles (Mach numbers 1.63 and 3.07) and their respective centerbodies were contoured to provide a smooth expansion to the design free-stream Mach number.

All model instrumentation and control lines and the engine propellant and coolant supply, bleed and return lines were run through the model and out the support spider into the plenum chamber. These lines, in turn, left the plenum chamber through a pressure-tight porthole to the various facility propellant, coolant, and instrumentation systems (Ref. 5).

Hydrogen gas (at 520°R), which simulated the prototype fuel rich turbine exhaust gases, was supplied from a common manifold having eight outlets to represent the eight propellant pumps; each outlet incorporated an orifice 0.055-in. in diameter for flow regulation. Hydrogen gas flow was initiated approximately three seconds after full chamber pressure was achieved. Hydrogen flow rates were calculated by measuring the pressure differential of six hydrogen supply tanks before and after a data run. Sufficient time was allowed after a data run for complete temperature recovery to assure a constant temperature process.

3.0 PROCEDURE

The nozzle inlet total pressure settings were determined from the desired simulated altitude at the nozzle exit and from the pressure ratio corresponding to the Mach number at which testing was performed. These pressure ratios were determined from the nozzle calibrations reported in Ref. 6. Nozzle inlet total temperature was maintained at 140°F ± 5° for Mach number 1.63 and at 200°F ± 5° for Mach number 3.07 testing.

Prior to each test period, the heat shield and flame shield were blackened by a fuel-rich oxyacetelyne torch to provide similar surface conditions for all runs.

A no-flow (static altitude tunnel conditions) data point was taken before each day's tests to determine if all pressure transducers were operating correctly and were giving repeatable data.

When steady flow conditions at the desired test altitude were established, the rocket firing sequence was initiated at a time designated t + O. A typical time history showing engine chamber pressure buildup is presented in Fig. 10.

"Engine-only" data were obtained after steady-state engine operation had been established and before the hydrogen flow was initiated.

The flow rate of hydrogen gas is referred to in this report in terms of heat ratio, which is the ratio of chemical heat content of the discharged hydrogen gas to the equivalent chemical heat content of the prototype missile turbine exhaust gases. Further definitions and the method of calculations are given in the Appendix. When hydrogen gas flow was equivalent to a heat ratio of 1.0, the flow momentum per unit area from the long overboard ducts was calculated to be approximately 100 percent of the prototype turbine exhaust momentum. The momentum per unit area for the streamlined duct was approximately 90 percent and for the short duct approximately 110 percent of the prototype turbine exhaust momentum.

4.0 RESULTS AND DISCUSSION

The Saturn SA-1 Booster afterbody was tested at Mach numbers 1.63 (33,000 to 45,000-ft altitude) and 3.07 (70,000 to 80,000-ft altitude). Table 3 shows test conditions for each firing. The heat transfer to the base heat shield caused by recirculation of the engine exhaust is given, and the heat transfer to the flame shield calorimeters is presented as a function of calorimeter location. The base heat shield and flame shield pressure data are presented as a function of altitude.

The model exhausterator did not completely simulate the prototype exhausterator (see Fig. 5). The total effects of this difference in flow direction are not known.

4.1 BASE HEATING

4.1.1 Base Heat Shield

Examination of a typical temperature versus time plot made from the base calorimeter data shows a smooth exponential curve (Fig. 11) with no change in the trend of the curve at or after the time hydrogen flow was initiated, indicating no burning of the hydrogen gas in the base region. This was further substantiated by lack of any visible flame in the motion pictures taken of the base during engine operation. Although there was an indication that hydrogen may have recirculated into the base (this will be discussed later in this report), no burning occurred in the base region regardless of the turbine exhaust duct configuration, the free-stream Mach number, or the altitude at which testing was accomplished. Although no base burning occurred some base heating was present which was attributed to recirculation of hot rocket exhaust gases. These gases gave a maximum heat transfer rate to the base of approximately 4.0 Btu/ft^2-sec for the M = 1.63 and M = 3.07 tests. The minimum heat transfer rate of 2.5 Btu/ft^2-sec on the base occurred between the outboard engine nozzle and the skirt.

The results of flowing hydrogen from the turbine exhaust ducts indicate that the duct which was chosen as the optimum duct in the lower portion of the trajectory (as reported in Ref. 3) would also be satisfactory for that portion of the trajectory covered by this series of tests.

Because Ref. 7 stated that burning could occur up to Mach number 3.5 and/or 100,000 ft, factors which may have prevented base burning in these tests were analyzed.

Model scale effects were possibilities first considered. Two effects which were imposed by the scale of the model were the reduced time the recirculated gases remained in the base (stay time) and the decreased distance between nozzles. The reduced stay time decreased the time available to ignite the gas. The reduced distance between nozzles increased the possibilities of flame quenching (Ref. 7).

The nozzle inlet total temperature for the Mach number 3.07 testing was 660°R, whereas the inlet temperature for true altitude simulation was 1140°R. This difference in temperature may have been a contributing factor to no base burning.

It was also possible that the hydrogen/air ratio in the base region was not within the flammability limit for hydrogen gas. This is a rather

improbable assumption because the flammability limits of hydrogen to air mixtures are between 9 and 74 percent by volume (Ref. 8). However, such a possibility was evaluated by varying the amount of hydrogen flow from the turbine exhaust ducts. The amount of hydrogen was varied by increasing and decreasing the hydrogen pressure. Tests were made with hydrogen flows ranging from heat ratios of 0.55 to 1.25 with no indication of base burning.

Two other possibilities are those of flame quenching and ignition energy (Ref. 8). These two phenomena were treated as one because there would be considerable difficulty in attempting to separate them. Quenching and its possible effects on scale base heating are discussed in Ref. 7. The quenching distance is defined as the minimum opening through which flames in a given mixture at a given temperature and pressure can pass. The quenching distance is approximately inversely proportional to the product of the static pressure of the gas and the temperature of the unburned gas in the base region. Because in the case of the model the static pressure of the gas is a function of the base pressure, the pressure could not be altered. However, the temperature of the hydrogen gas at the exit of the turbine exhaust ducts was approximately 600°R lower than the temperature of the exhaust products at the exit of the full-scale ducts (520°R-1110°R). This temperature could be increased without sacrifice of any simulation already obtained. The hydrogen gas was therefore heated by an immersion-type heat exchanger so that the temperature at the exit of the turbine exhaust duct was approximately 800°R. Heating of the hydrogen has several effects on the gas properties; it increases the flammability limits of the hydrogen, it decreased the quenching distance, and it decreases the ignition energy required (Ref. 8). All three effects were desirable because they all would increase the possibilities of base burning, but the combined effects were not sufficient to cause burning in the model base region.

4.1.2 Flame Shield

Figure 12 is a typical heat transfer versus calorimeter temperature plot. These data were extrapolated to obtain the values of heat transfer rate presented in Fig. 13. The data were extrapolated to the starting temperature of the calorimeter and are presented as the maximum heat transfer rate. This extrapolation to the starting temperature was chosen because according to the equation $\dot{q} = h_c A(T_g - T_w)$, the maximum heat transfer occurs where $(T_g - T_w)$ is a maximum (assuming T_g and h_c constant); therefore, the heat transfer would be the greatest at the start of a given run when T_w is a minimum.

The heat transfer on the flame shield (Fig. 13) at Mach number 1.63 indicates a maximum rate of 113 Btu/ft^2-sec and occurred at the calorimeter located in the center of the flame shield. The minimum rate of heat transfer was 47 Btu/ft^2-sec and occurred at the calorimeter located the greatest distance from the center of the flame shield. The Mach number 3.07 data indicated a maximum heat transfer rate of 72 Btu/ft^2-sec to the calorimeter located in the center of the flame shield, whereas the minimum heat transfer rate was an average of 44 Btu/ft^2-sec to the third calorimeter from the center of the flame shield. With one inboard engine inoperative the heat transfer to the flame shield was 15 Btu/ft^2-sec to the calorimeter located in the center of the flame shield (Fig. 13). This decrease in heat transfer was as predicted in Ref. 1.

The film heat transfer coefficient was calculated by the methods presented in the Appendix. The two methods showed good agreement, and the results are presented in Fig. 14.

The calculated values of heat transfer coefficient indicated a maximum coefficient at the center calorimeter of the flame shield and decreased to a minimum coefficient at the calorimeter located the greatest distance from the center of the flame shield. This profile was determined for both Mach numbers 1.63 and 3.07 testing. For Mach number 1.63 testing, the average coefficients were 0.227 Btu/ft^2-sec°F and 0.066 Btu/ft^2-sec°F, whereas for Mach number 3.07, the average coefficients were 0.143 Btu/ft^2-sec°F and 0.059 Btu/ft^2-sec°F.

4.2 BASE PRESSURE

4.2.1 Base Heat Shield Pressure

Base pressure data presented in this report were obtained from an arithmetical average of the seven base pressure taps located as shown in Fig. 8a. In general, the variation in the individual base pressures was within ±5 percent of the average base pressure.

The variations of base to free-stream pressure ratio and of base pressure coefficient with altitude are shown in Figs. 15 and 16. The data at 41,000 ft are from M = 1.63 test (except as noted), and the data at the 75,000-ft level are from Mach number 3.07 tests. Trajectory altitude for Mach number 3.07 could not be obtained because of pressure ratio limitations, but a number of tests were run at lower altitudes to establish a trend whereby an estimated base pressure might be obtained. A number of "off trajectory" runs were also made at Mach number 1.63.

The data presented were those obtained with hydrogen discharging from all eight turbine exhausts. The base pressure rise at the time of hydrogen initiation was approximately 0.05 psia for all ducts. Because no base burning occurred at any altitude or Mach number, no large base pressure rise would be expected with the initiation of hydrogen flow.

The base pressure data show a small but distinct difference between various overboard ducts which is attributed to difference in aerodynamic characteristics and not to the difference in amount of recirculated hydrogen as the base pressure rose approximately 0.05 psia when hydrogen was initiated. This difference is more noticeable as a base pressure coefficient in Fig. 16 than as a pressure ratio.

The trend of both the base pressure ratio and base pressure coefficient data indicates an increase as altitude increases. Several data points from Ref. 9 are shown in both Figs. 15 and 16. The reference data points agree quite well with the trend as shown with the exception of $M_\infty = 1.4$ base pressure coefficient which indicates that this trend may change between $M_\infty = 1.4$ and $M_\infty = 1.5$. This indication of trend change is also shown in Ref. 9.

The base pressure was affected very little when an inboard engine was inoperative (see Figs. 15 and 16). It should be noted, however, that the pressures were measured on the side of the base opposite the inoperative inboard engine.

4.2.2 Flame Shield Pressure

The flame shield data presented were obtained from the one static pressure tap in the shield (Fig. 8b). Flame shield data are presented as a ratio of flame shield pressure to base pressure. This ratio was used in preference to the ratio with free-stream pressure because the gases from the flame shield region exhaust into the base region and therefore are dependent on, or influenced by, the base pressure.

The flame shield pressure data indicated an average pressure of 2.87 psia for all runs for both Mach numbers 1.63 and 3.07. This flame shield pressure ratioed to base pressure indicated a value greater than 1.79 (critical pressure ratio, see the Appendix) for all Mach number 3.07 tests and is shown in Fig. 17. The ratio for the Mach number 1.63 test (in the 41,500-ft-altitude range) is less than critical (about 1.4) and is also shown in Fig. 17. An extrapolation to a pressure ratio of 1.8 of the Mach number 3.07 data indicates that the flame shield to base pressure ratio would become critical at about 63,000 ft.

Several tests were made at both M_∞ = 1.63 and M_∞ = 3.07 with one inboard engine inoperative. The flame shield pressure in both cases (Fig. 17) showed a marked decrease when compared with that taken with all eight engines operating. This is attributed to the fact that the area available for the rejected gas to escape was greatly increased while the amount of rejected gases was decreased (Ref. 1). The flame shield pressure was approximately equal to the base pressure at Mach number 1.63 and was only slightly higher than the base pressure at Mach number 3.07 as indicated in Fig. 17.

5.0 SUMMARY OF RESULTS

The results obtained during an investigation of base heating with a 5.47-percent-scale model of the SA-1 Saturn booster afterbody at Mach number 1.63 altitudes of 33,000 to 45,000 ft and a Mach number 3.07 at altitudes of 70,000 to 80,000 ft are summarized as follows:

1. No burning of the hydrogen, which simulated the turbine exhaust products, occurred in the base at either Mach number 1.63 or 3.07.
2. Maximum heat transfer to the base was approximately 4.0 Btu/ft^2-sec with minimum values of 2.5 Btu/ft^2-sec in the region between the rocket nozzles and skirt extensions.
3. The heat transfer rate to the flame shield at Mach number 1.63 was 113 Btu/ft^2-sec at the center calorimeter and decreased to 47 Btu/ft^2-sec at the calorimeter located the greatest distance from the center of the flame shield. At Mach number 3.07, the heat flux was 72 Btu/ft^2-sec at the center calorimeter and decreased in value to 44 Btu/ft^2-sec at the third calorimeter from the center.
4. A profile of calculated values of film heat transfer coefficient for the flame shield indicated the maximum at the center and the minimum at the greatest distance from the center. At Mach number 1.63, data indicated the average maximum value was 0.227 Btu/ft^2-sec°F, and the average minimum value was 0.066 Btu/ft^2-sec°F, whereas at Mach number 3.07 the average maximum value was 0.143 Btu/ft^2-sec°F, and the average minimum value was 0.059 Btu/ft^2-sec°F.

5. Base pressure data indicated a slight increase, when hydrogen flow was initiated, with all duct configurations evaluated.

6. There was little effect on base pressure during operation with an inoperative inboard engine.

7. Flame shield pressure measured near the center of the shield was constant at approximately 2.87 psia for all testing with eight engines operating.

8. An extrapolation of the Mach number 3.07 data to a pressure ratio of 1.79 indicates that the flame shield to base pressure ratio would become critical at about 63,000 ft.

9. The flame shield pressure with one inboard engine inoperative was equal to the base pressure at Mach number 1.63 and was 15 percent higher than base pressure at Mach number 3.07.

REFERENCES

1. Goethert, B. H. "Base Flow Characteristics of Missiles with Cluster Rocket Exhaust." Institute of Aerospace Science Paper No. 60-89, July 1960.

2. Goethert, B. H. "Base Heating Problems of Missiles and Space Vehicles." American Rocket Society Paper No. 1666-61, March 1961.

3. Parker, Joseph R. and Gillard, T. J. "An Investigation of Base Heating with a 5.47-Percent Saturn SA-1 Booster Model at Mach Numbers 0.8 and 1.15." AEDC-TN-61-134, November 1961.

4. Westkaemper, J. C. "An Analysis of Slug-Type Calorimeters for Measuring Heat Transfer from Exhaust Gases." AEDC-TN-60-202, November 1960.

5. Test Facilities Handbook, (3rd Edition). "Rocket Test Facility, Vol. 2." Arnold Center, January 1961.

6. Peters, C. E. "Annular Nozzles for Missile Base Flow Testing." AEDC-TN-60-62, May 1960.

7. Dahm, Werner K. and Wilson, Homer B., Jr. "Some Preliminary Results of the Saturn Base Heating Program." George C. Marshall Space Flight Center. Paper presented at Rocket Testing Symposium, Arnold Engineering Development Center, Tullahoma, Tennessee, June 28-29, 1961.

8. Drell, Isadore L. and Belles, Frank E. "Survey of Hydrogen Combustion Properties." NASA Report 1383, 1958.

9. Kennedy, T. L. and Lowry, J. F. "An Investigation of Base Heating on a 5.47-Percent Scale Model of the Saturn S-1 Booster at Transonic Mach Numbers." AEDC-TN-61-106, August 1961.

APPENDIX

METHODS OF CALCULATION

HEAT TRANSFER

Total heat transfer ($\dot{q}$) was computed for each calorimeter from the indicated calorimeter temperature rise over each 0.6-sec interval and using:

$$\dot{q} = \frac{c_p m}{A} \times \frac{dT}{dt}$$

where A = Calorimeter slug exposed surface area, ft^2

$\frac{dT}{dt}$ = Temperature derivative with respect to time, °F/sec

BASE PRESSURE

Base pressure (p_B) data presented in this report were obtained by averaging the values from the seven static pressure taps located on the base. Flame shield pressure (p_{FS}) data were obtained from the static pressure tap located on the flame shield. Base pressure coefficient was calculated from:

$$C_p = (p_B - p_\infty)/q_\infty$$

where

$$q_\infty = 1/2\ p_\infty\ \gamma\ M_\infty^2$$

HEAT RATIO

Gaseous hydrogen was used to simulate the combustible turbine exhaust gases of the prototype system. Hydrogen was selected because of its wide flammability limits (9 to 74-percent hydrogen to air, by volume - Ref. 8) and was discharged at a rate which simulated the heat content that would be available (equivalent heat content):

1. If the turbine exhaust gases discharged from the model were of the same chemical composition as those of the prototype
2. If these gases were discharged from the model in the same proportion to model engine total propellant flow as the gases from the prototype
3. If a combustion efficiency of 100 percent were assumed for burning of the turbine exhaust gases.

Based on these assumptions, the turbine exhaust flows in this investigation were referred to in terms of heat ratio calculated as follows:

Given:
1. Total prototype propellant flow = 643 lb/sec/engine
2. Total prototype turbine exhaust gas flow = 13.25 lb/sec/engine
3. 57 percent of prototype turbine exhaust gas flow is unburned RP-1 with a heating value = 18,600 Btu/lb
4. Total model propellant flow = 2.22 lb/sec/engine
5. Lower heating value of gaseous hydrogen = 51,600 Btu/lb

Therefore, the ratio of prototype total propellant flow to combustible turbine exhaust gas flow = $\frac{643}{13.25 \times 0.57}$ = 85.1.

To maintain the model flow ratio at this value would require 2.22/85.1 = 0.0261 lb/sec of unburned RP-1, with an available heat rate of 0.0261 x 18,600 = 485 Btu/sec. To obtain this heat rate with hydrogen gas a flow of 485/51,600 = 0.0094 lb/sec would be required. Heat ratio was then defined as the actual hydrogen flow rate during each particular run divided by 0.0094.

FILM HEAT TRANSFER COEFFICIENT

There are several suggested methods for calculating film heat transfer coefficient when only calorimeter temperature and calculated values of heat transfer are available. Two of these methods are given below:

1. Reference 4 suggests assuming h_c and T_g constant and combining $h_c A (T_g - T_w) = m_{cp} \frac{dT}{dt} = \dot{q}$ in which h_c and T_g are unknown, and all other values are found experimentally and then solving by using measured values of $\dot{q}$ at two different times. The two best points are those near the beginning and near the end of the steady-state test conditions.
2. Reference 9 suggests that the $\dot{q}$ vs T data (Fig. 12) may be extrapolated to a heat transfer rate of zero thereby obtaining an equilibrium temperature and assuming this to be the gas temperature. This gas temperature may then be used in $\dot{q} = h_c A (T_g - T_w)$.

CRITICAL PRESSURE RATIO

The ratio of specific heats for the products of combustion for the LOX, RP-1 propellant was estimated to be approximately 1.23. This value was used to determine the critical pressure ratio of 1.79(P_{FS}/P_B) for the gases in the flame shield region.

The following equation was used for this calculation:

$$\frac{P_{FS}}{P_B} = \left(1 + \frac{\gamma - 1}{2} M^2\right)^{\frac{\gamma}{\gamma - 1}}$$

since M = 1

$$\frac{P_{FS}}{P_B} = \left(\frac{\gamma + 1}{2}\right)^{\frac{\gamma}{\gamma - 1}}$$

TABLE 1

ROCKET ENGINE DESIGN DATA

	Model	Prototype
Nozzle Shape	Contoured	Contoured
Nozzle Throat Diameter, in.	0.90	16.5
Nozzle Exit Diameter, in.	2.50	46.74
Nozzle Area Ratio	7.72	8.0
LO_2 Flow, lb/sec/engine	1.5 lb/sec	441
RP-1 Flow, lb/sec/engine	0.7 lb/sec	202
Chamber Pressure, psia	500 psia	575
Thrust Chamber and Nozzle Coolant Flow Rate, lb/sec	Water 3 lb/sec	Regenerative Fuel Cooled

TABLE 2

INSTRUMENTATION SUMMARY

Parameter	Method of Measurement	Method of Recording	Range	Response Time, millisec	Max Deviation, ± Percent of Full Scale
Calorimeter Temperature	C/A Thermocouple	Magnetic Tape	0-1800 °F	50.0	1.0
Base Pressure	Strain-Gage Transducer	Magnetic Tape	0-10 psia	50.0	0.75
Base Pressure	Strain-Gage Transducer	Oscillograph	0-10 psia	50.0	2.5
Free-Stream Pressure	Strain-Gage Transducer	Magnetic Tape	0-15 psia	50.0	0.75
Combustion Chamber Pressure	Strain-Gage Transducer	Continuous Inking Recorder	0-1000 psig	500	2.0
Injector Pressure	Strain-Gage Transducer	Continuous Inking Recorder	0-1000 psig	500	2.0
Propellant Flows	Turbine-Type Flowmeter	Oscillograph	0-1.5 lb/sec	5.0	0.5

TABLE 3

SUMMARY OF CONDITIONS FOR INDIVIDUAL TEST FIRINGS

Mach Number 1.63

Run No.	Altitude	O/F Ratio	Heat Ratio	Remarks
3-02	42,500	1.71	1.05	Long Duct Structural Bracket
3-04	42,400	2.13	1.04	" " " "
4-02	45,500	2.29	0.98	" " " "
4-04	45,500	2.37	0.93	" " " "
6-04	41,750	2.34	1.03	" " " "
6-06	41,750	2.26	0.93	" " " "
9-02	41,600	1.72	0.88	" " " "
9-04	41,600	1.71	1.01	" " " "
10-02	41,500	2.21	1.14	" " " "
10-04	41,500	2.23	1.06	" " " "
11-02	41,500	2.40	0.96	" " " "
11-04	41,600	2.35	0.95	" " " "
12-02	41,600	2.19	0.92	Short Duct
12-04	41,600	2.19	0.97	" "
14-02	41,600	2.31	0.56	Long Duct Airfoil Bracket
14-04	41,750	2.39	0.88	Streamlined Duct Hydrogen Heater
14-06	41,750	2.47	1.22	" " " "
15-02	42,200	2.72	0.58	" " " "
15-04	42,200	2.20	0.89	" " " "
15-06	42,300	2.18	0.51	" " " "
16-02	42,000	2.07	0.86	" " " "
16-04	42,200	1.67	0.83	" " " "
17-02	31,500	2.22	0.73	" " " "
17-04	31,500	2.05	0.57	" " " "
17-06	31,500	1.66	0.75	" " " "
18-02	42,100	2.15	0.81	" " " "
18-04	42,100	1.72	0.75	" " " "
18-06	42,100	1.72	0.0	No Hydrogen
19-02	42,100	2.07	1.07	Exhausterators Only
19-04	42,100	1.96	1.15	" "
19-06	42,200	1.62	1.07	" "
20-04	42,100	2.32	0.96	Long Duct Airfoil Bracket Inboard Engine Out
20-06	42,100	2.26	0.94	Long Duct Airfoil Bracket Inboard Engine Out

TABLE 3 (Concluded)

Mach Number 3.07

Run No.	Altitude	O/F Ratio	Heat Ratio	Remarks
10-02	75,000	2.07	1.16	Long Duct Airfoil Bracket
11-02	75,000	2.11	1.16	" " " "
11-04	78,000	2.11	1.06	" " " "
12-02	75,000	2.14	1.03	" " " "
13-02	75,000	1.84	1.04	" " " "
13-04	75,000	2.36	0.99	" " " "
13-06	70,000	2.09	1.19	" " " "
13-08	80,000	2.08	1.27	" " " "
14-02	75,000	1.97	1.01	Short Duct
14-04	75,000	1.98	1.06	" "
14-06	75,000	2.02	1.01	Streamlined Duct
14-08	75,000	2.02	1.08	" "
15-02	75,000	2.13	0.99	Long Duct Structural Bracket
15-04	75,000	2.12	1.07	" " " "
16-02	75,000	2.14	0.99	Long Duct Airfoil Bracket Inboard Engine Out
16-04	75,000	2.01	0.96	Long Duct Airfoil Bracket Inboard Engine Out

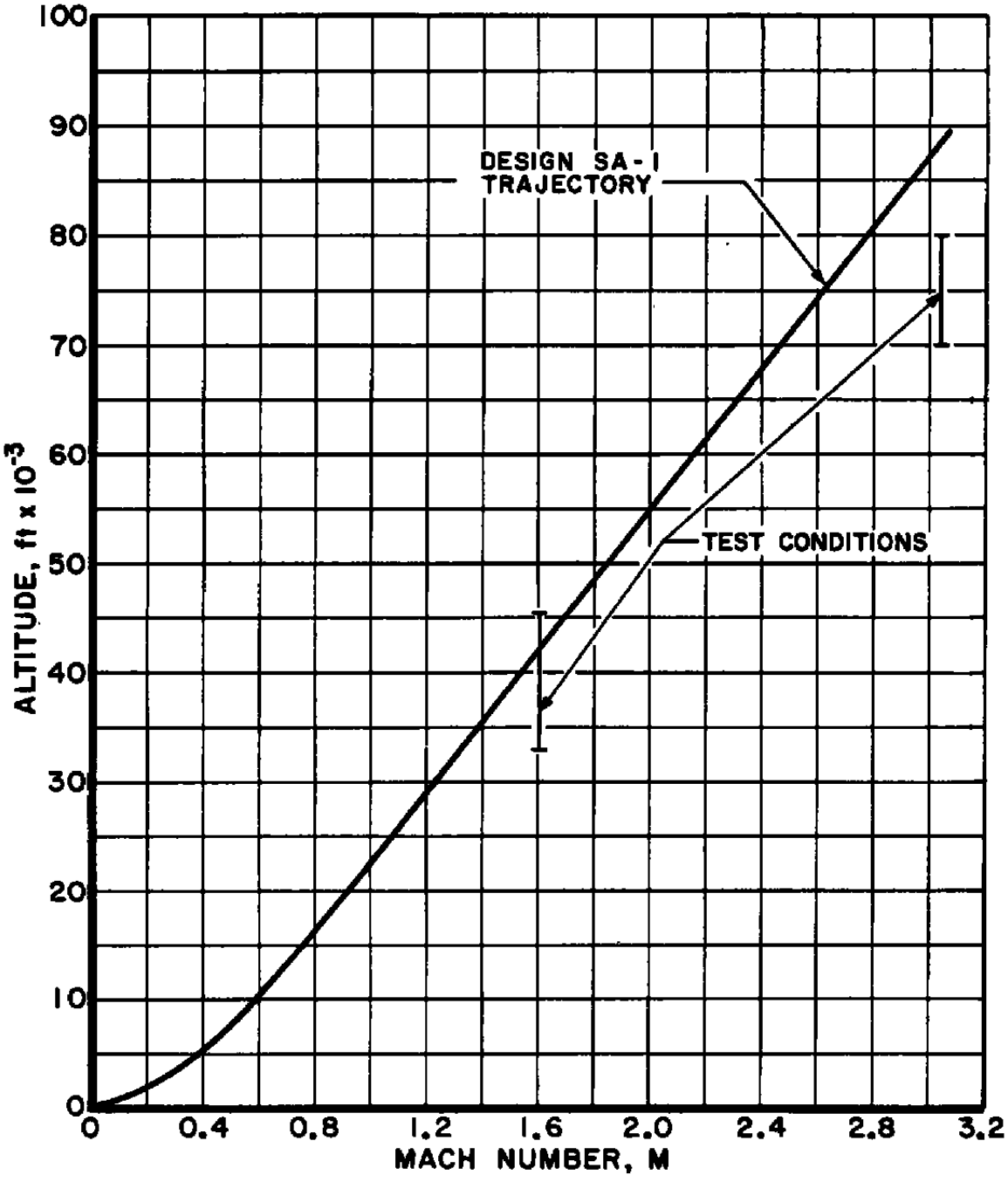

Fig. 1 Design Trajectory

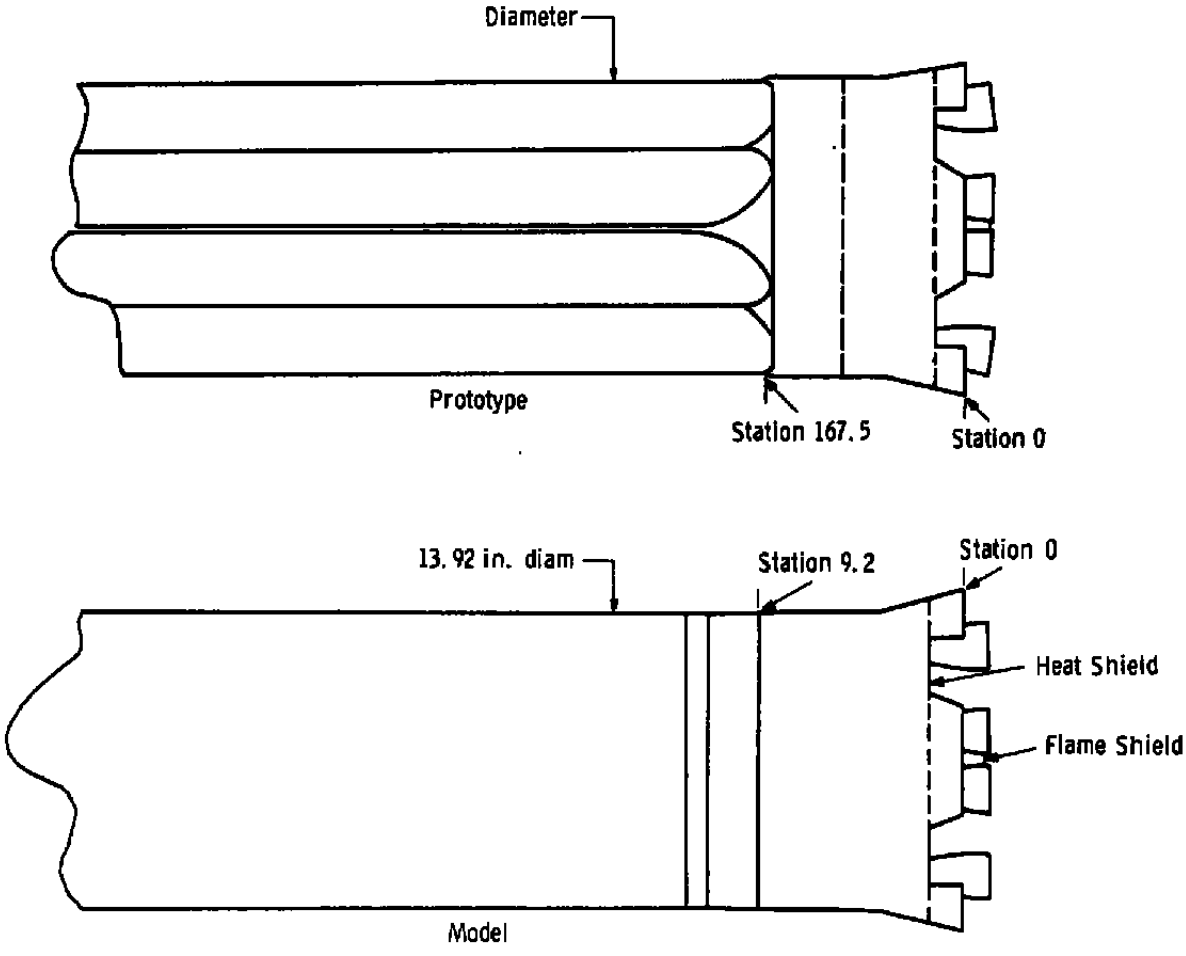

Fig. 2 Comparison of Model External Shroud Contour with Prototype

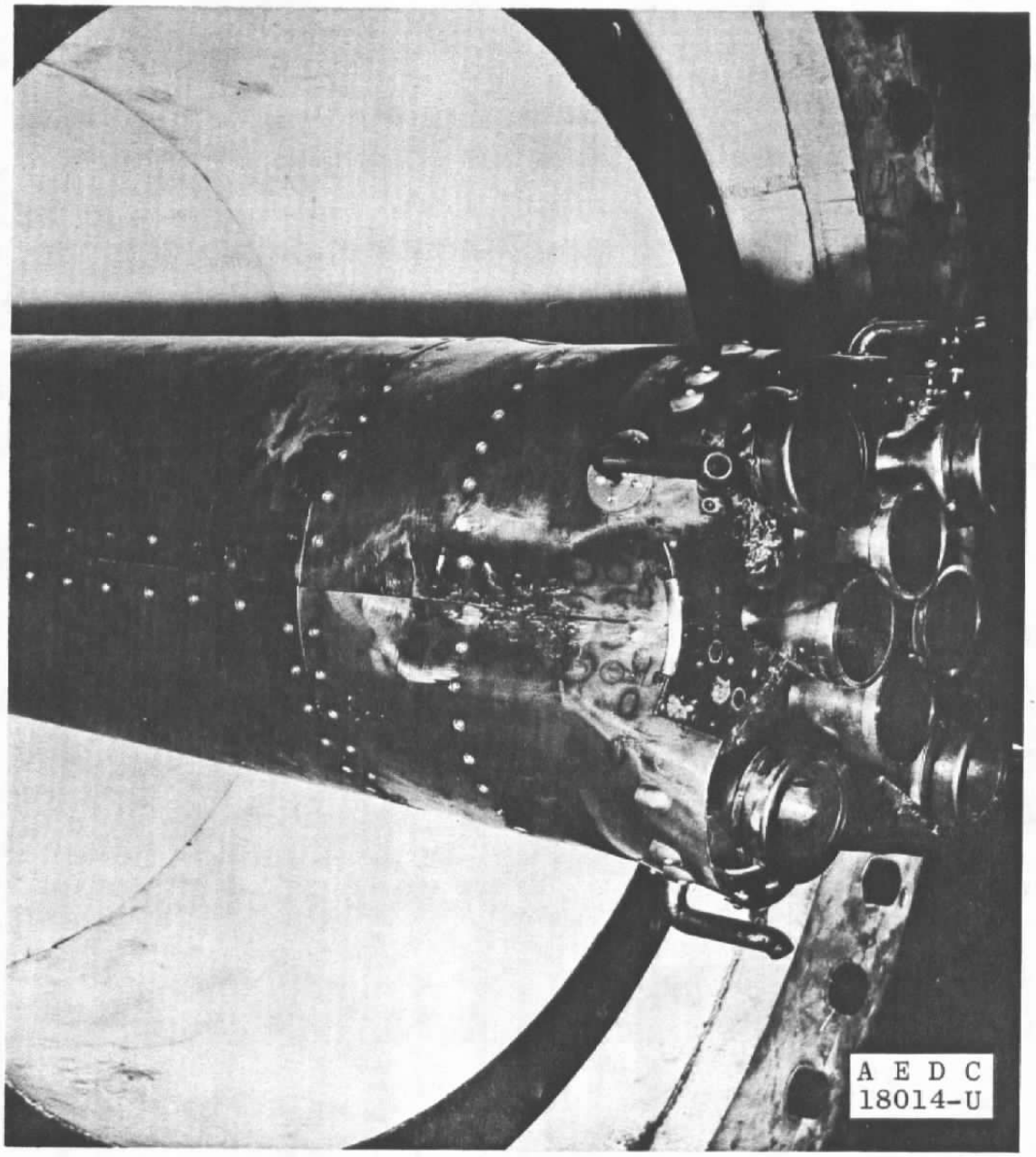

a. Three-Quarter Left View of Long Duct Configuration

Fig. 3 Views of the 5.47-Percent Saturn Model

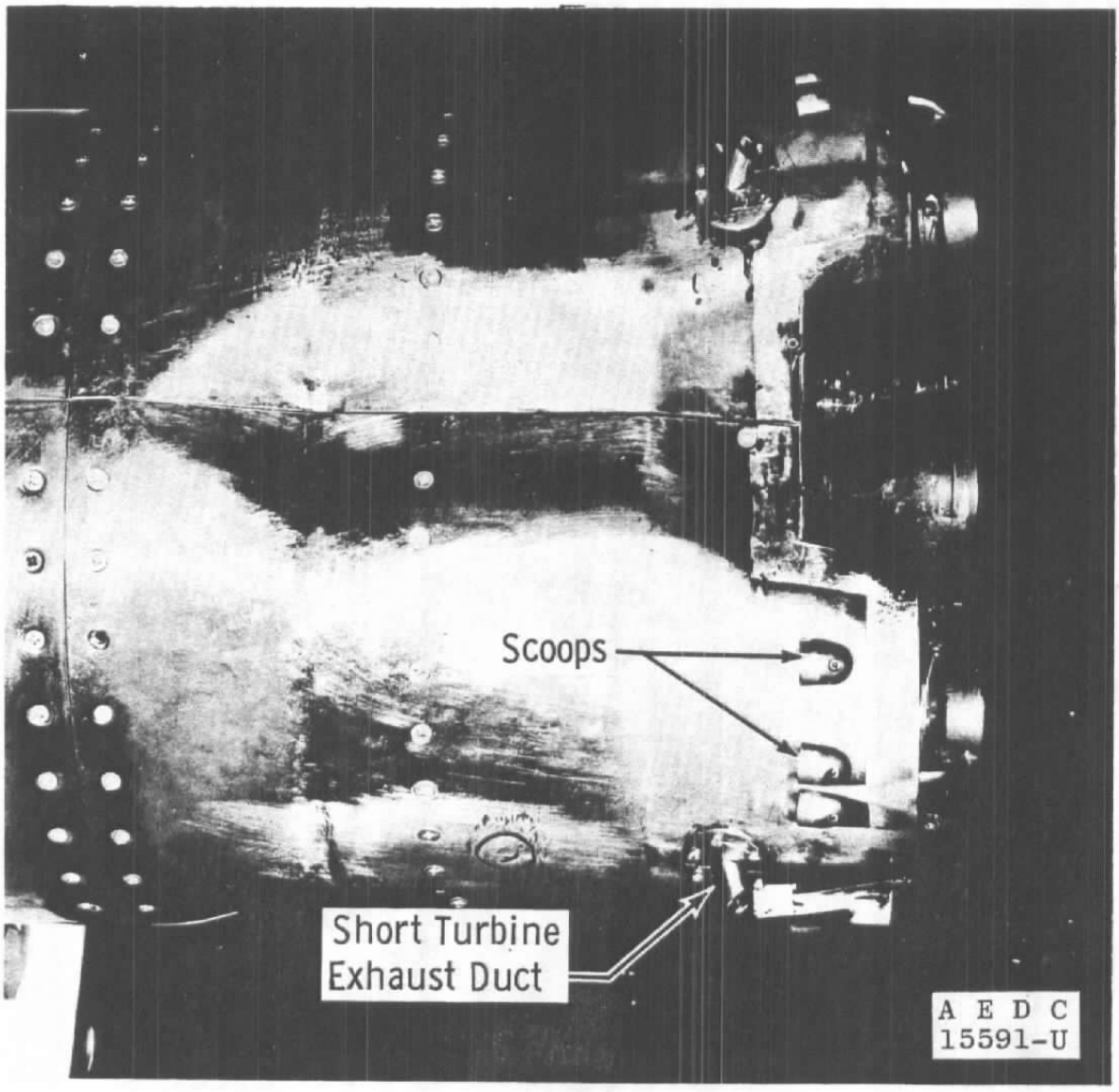

b. Side View of Short Duct Configuration

Fig. 3 Continued

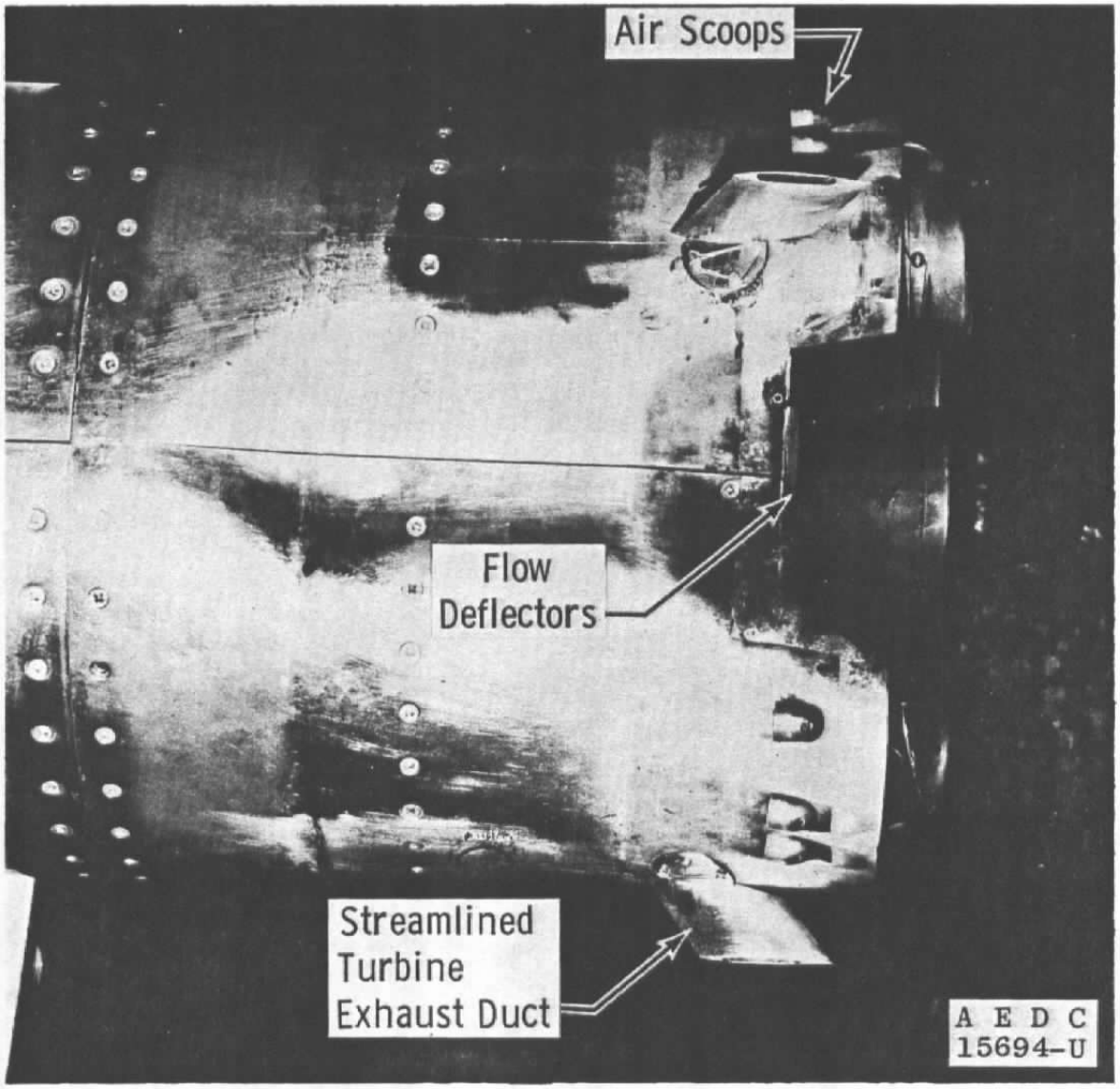

c. Side View of Streamlined Duct Configuration

Fig. 3 Continued

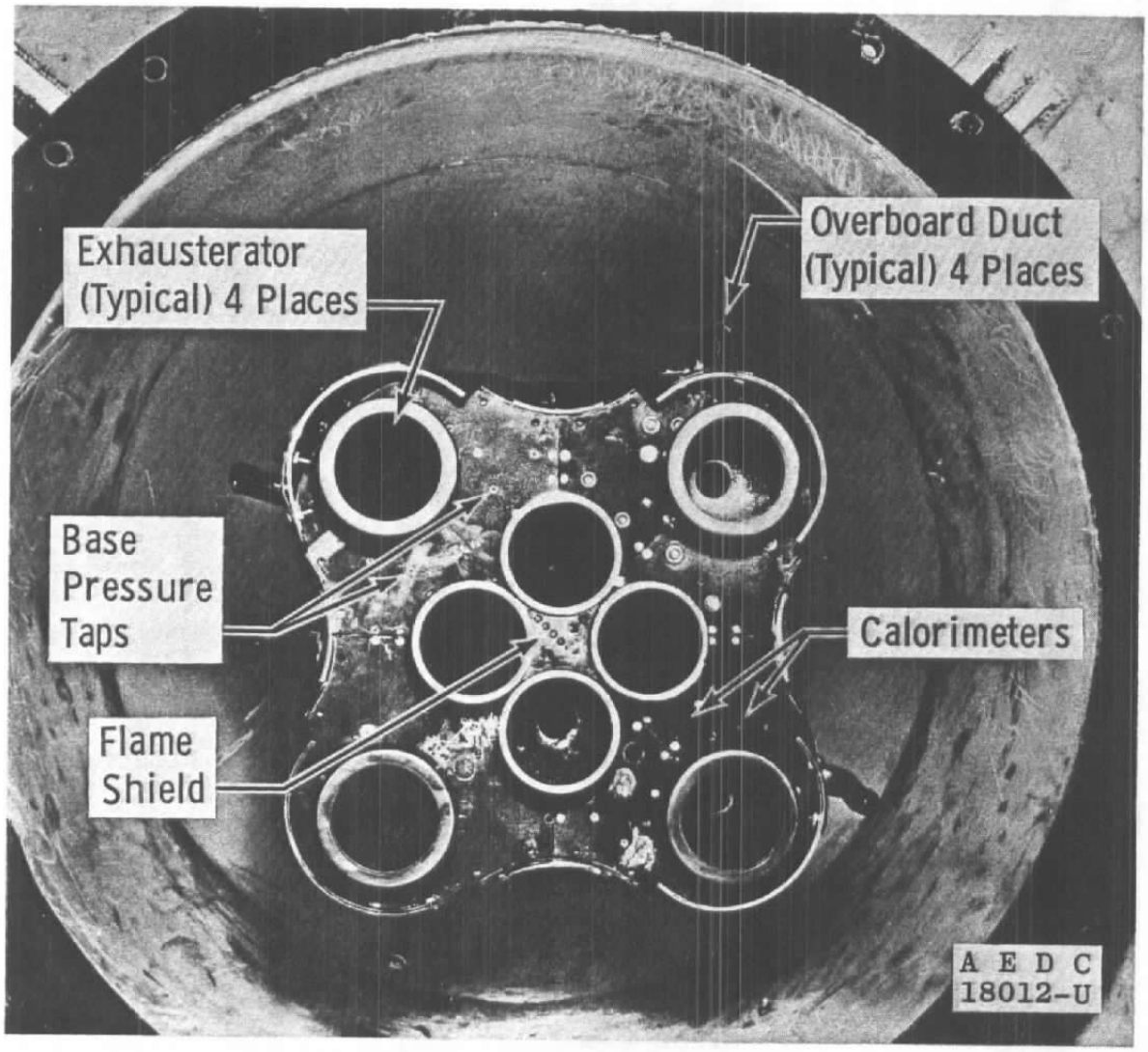

d. Rear View

Fig. 3 Concluded

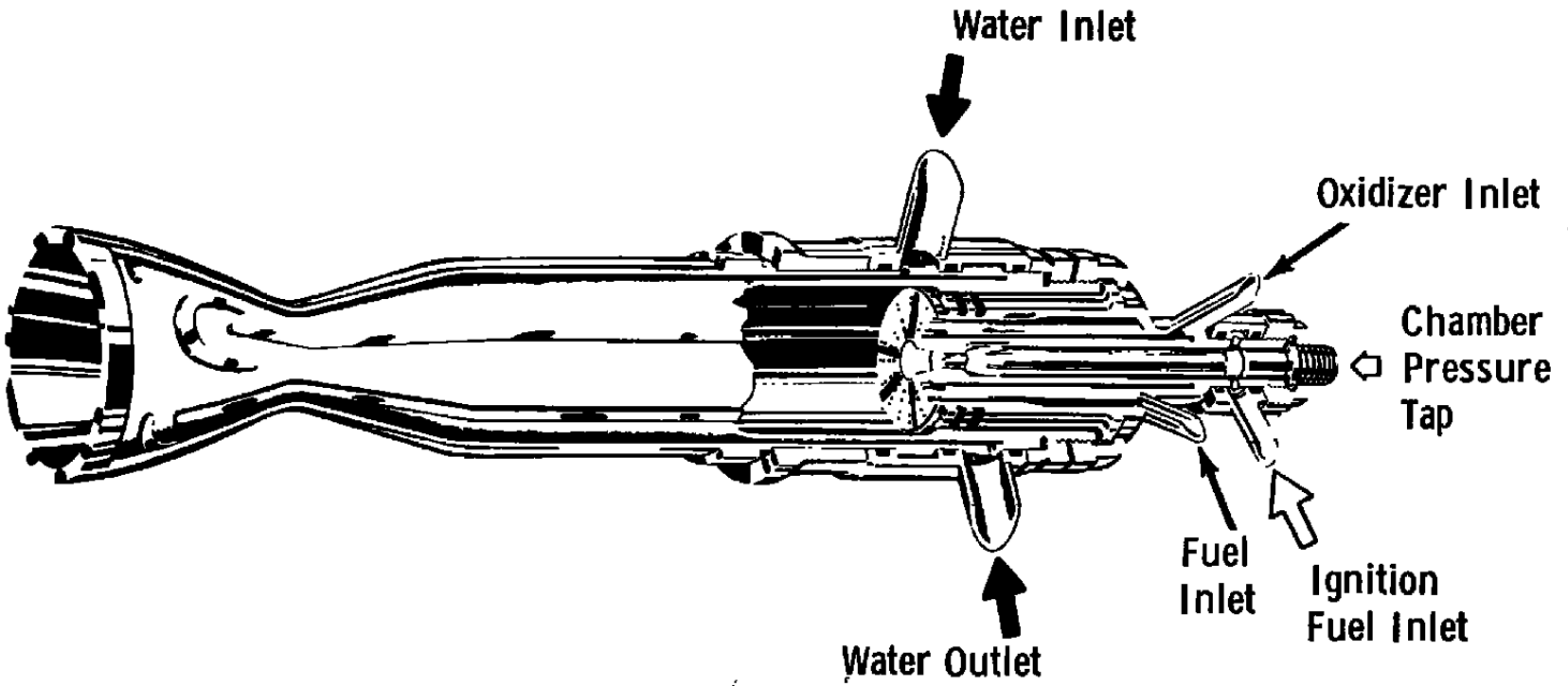

Fig. 4 Cutaway View of Model Engine

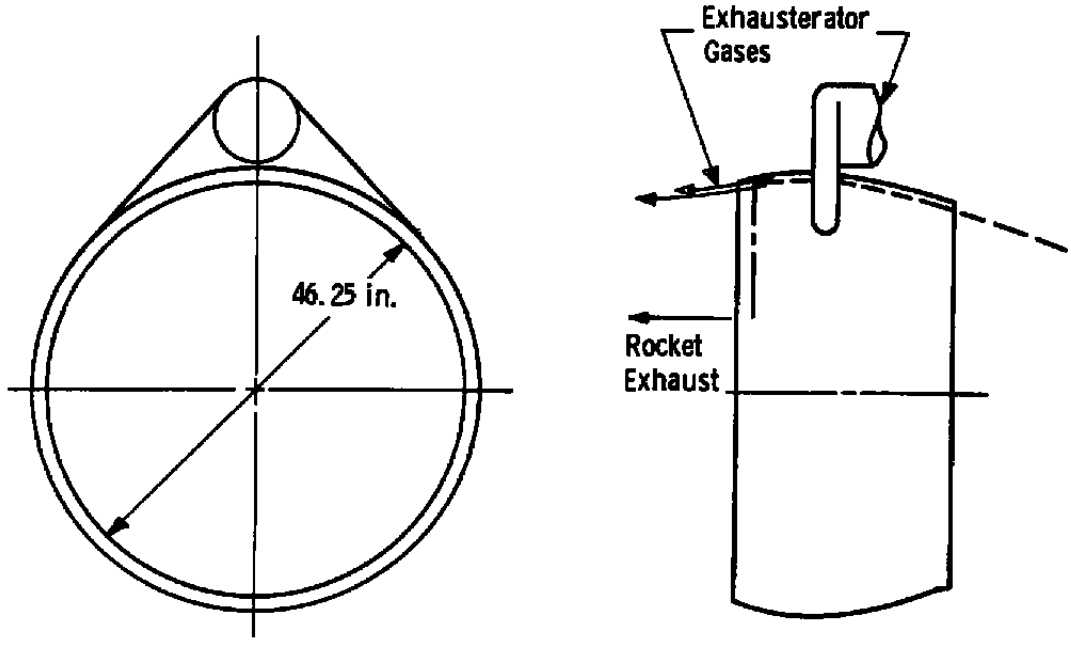

Exhausterator for Prototype Engines

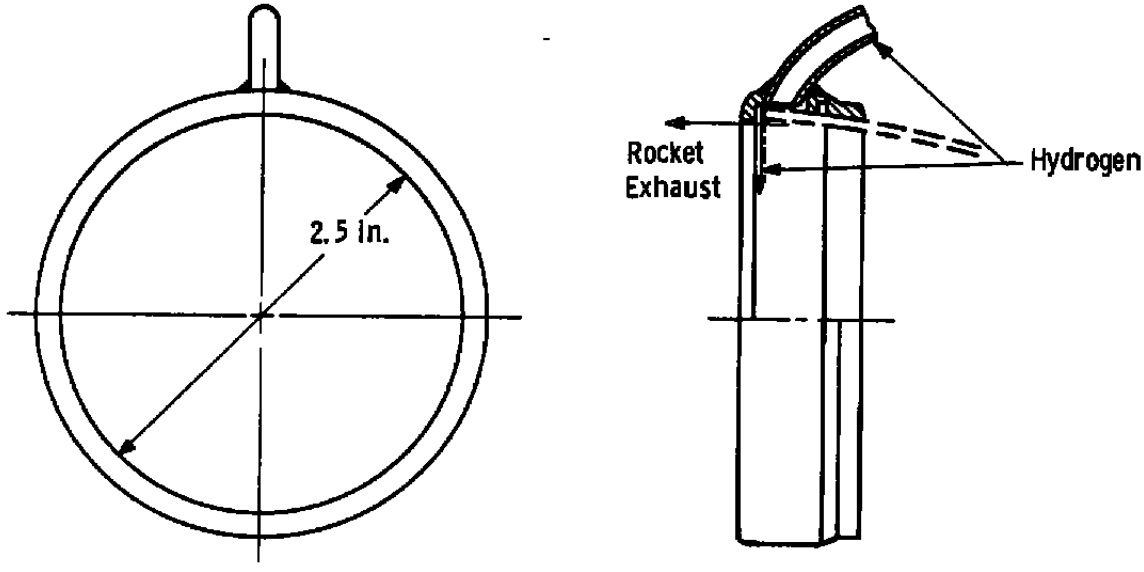

Exhausterator for Model Engines

Fig. 5 Comparison of Model Exhausterator Design with Prototype

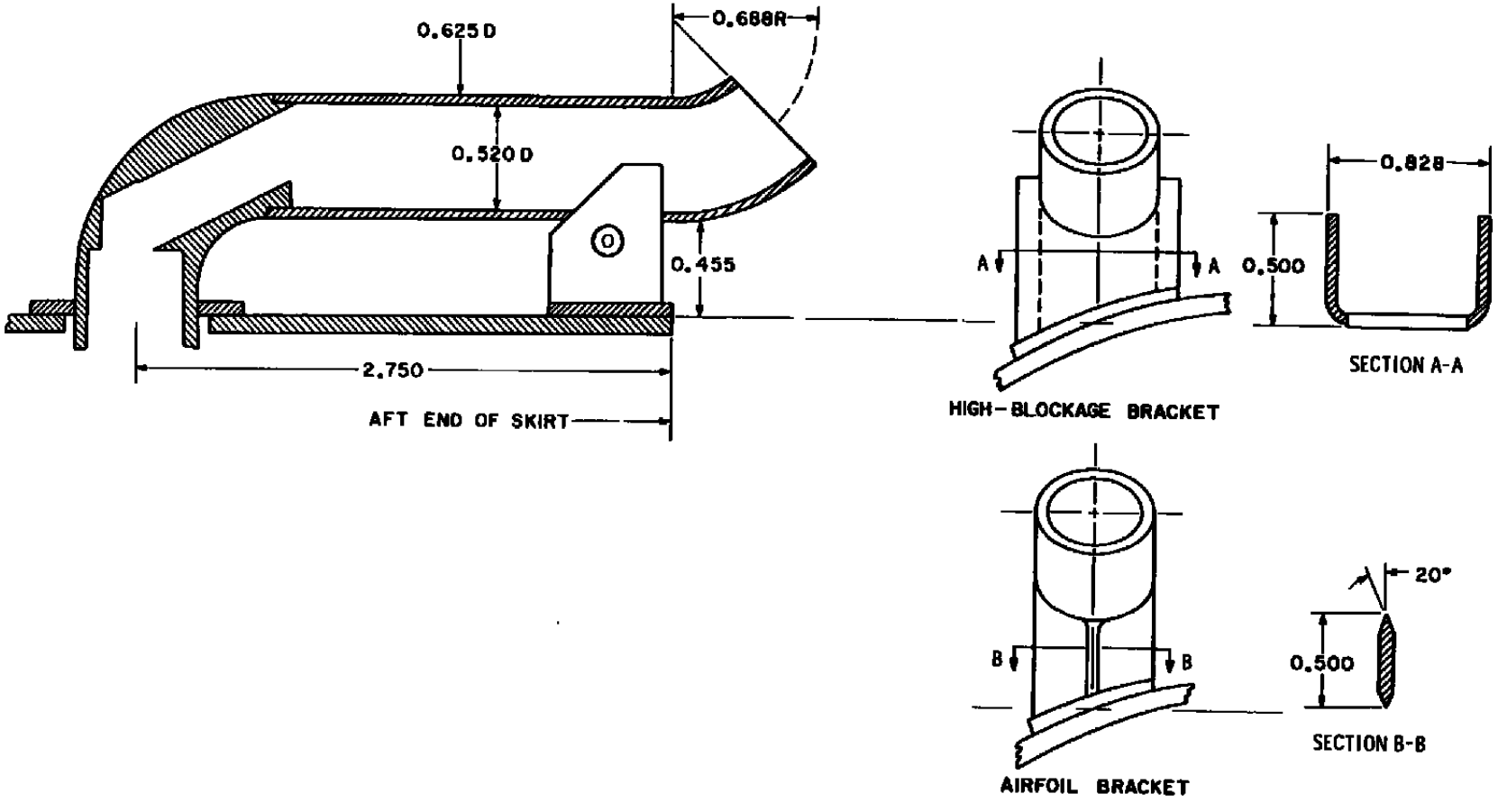

a. Long Duct Configuration

Fig. 6 Details of Model Overboard Turbine Exhaust Duct Configuration

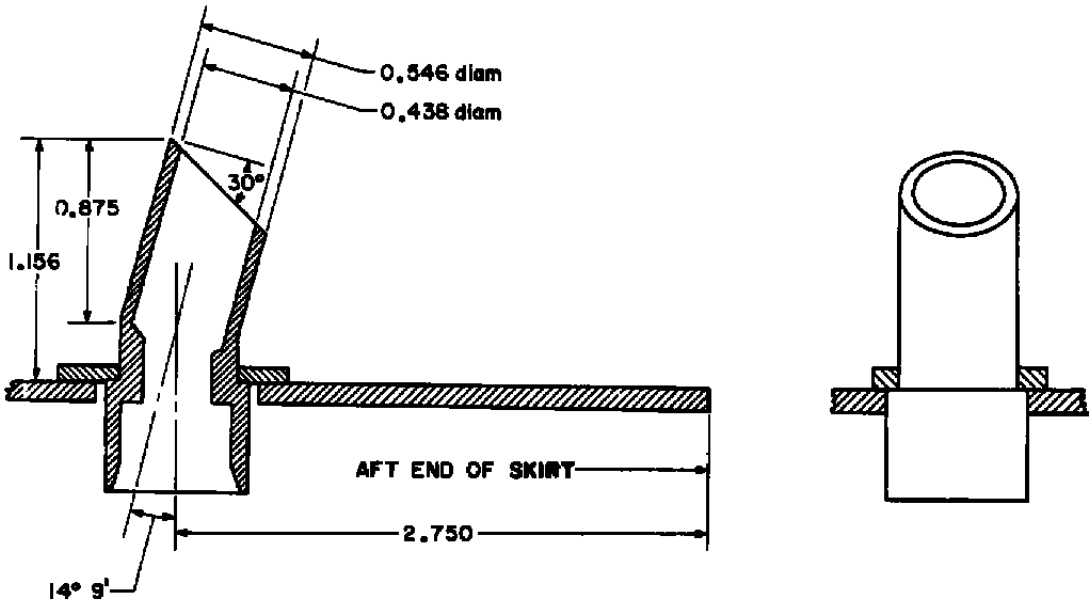

b. Short Duct Configuration

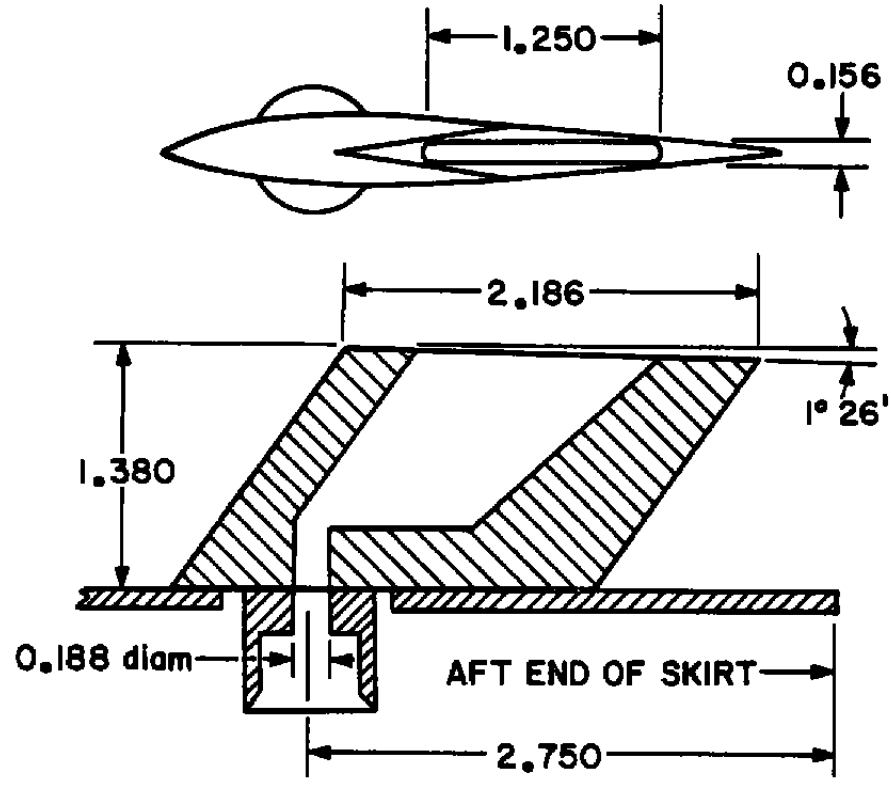

c. Streamlined Duct Configuration

Fig. 6 Concluded

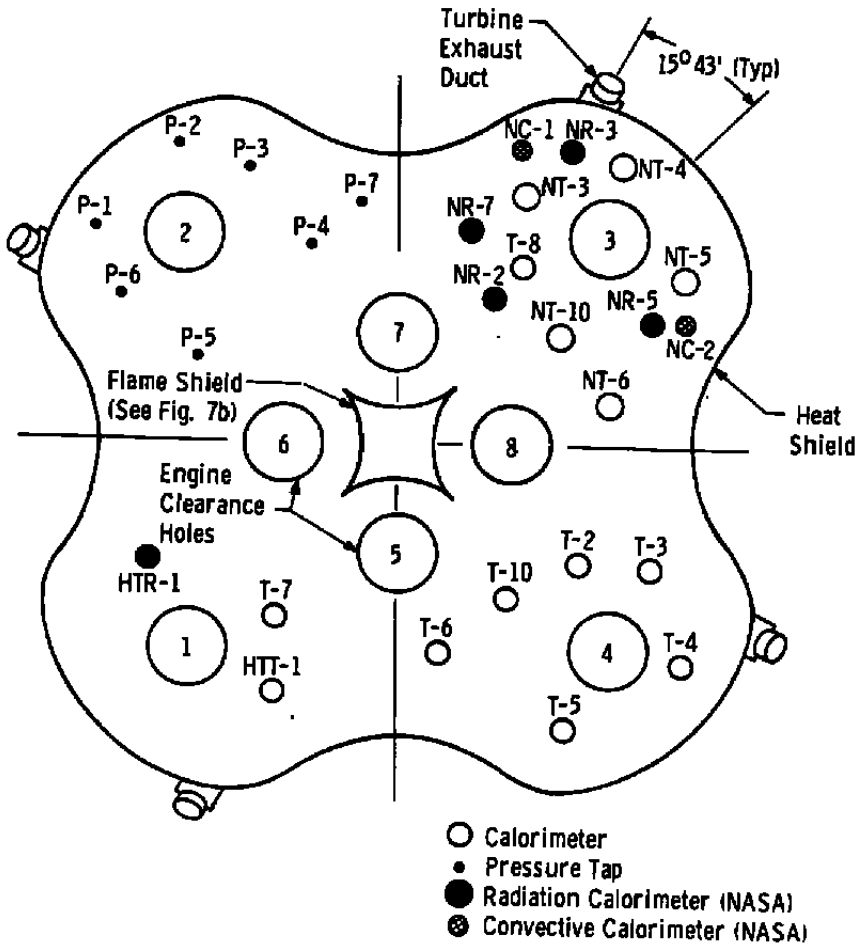

a. Heat Shield

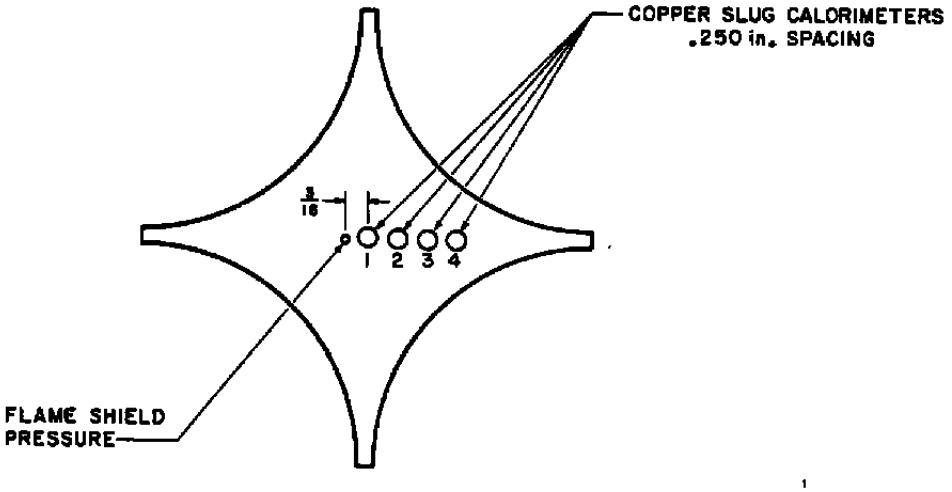

b. Flame Shield

Fig. 7 Location of Heat and Flame Shield Instrumentation

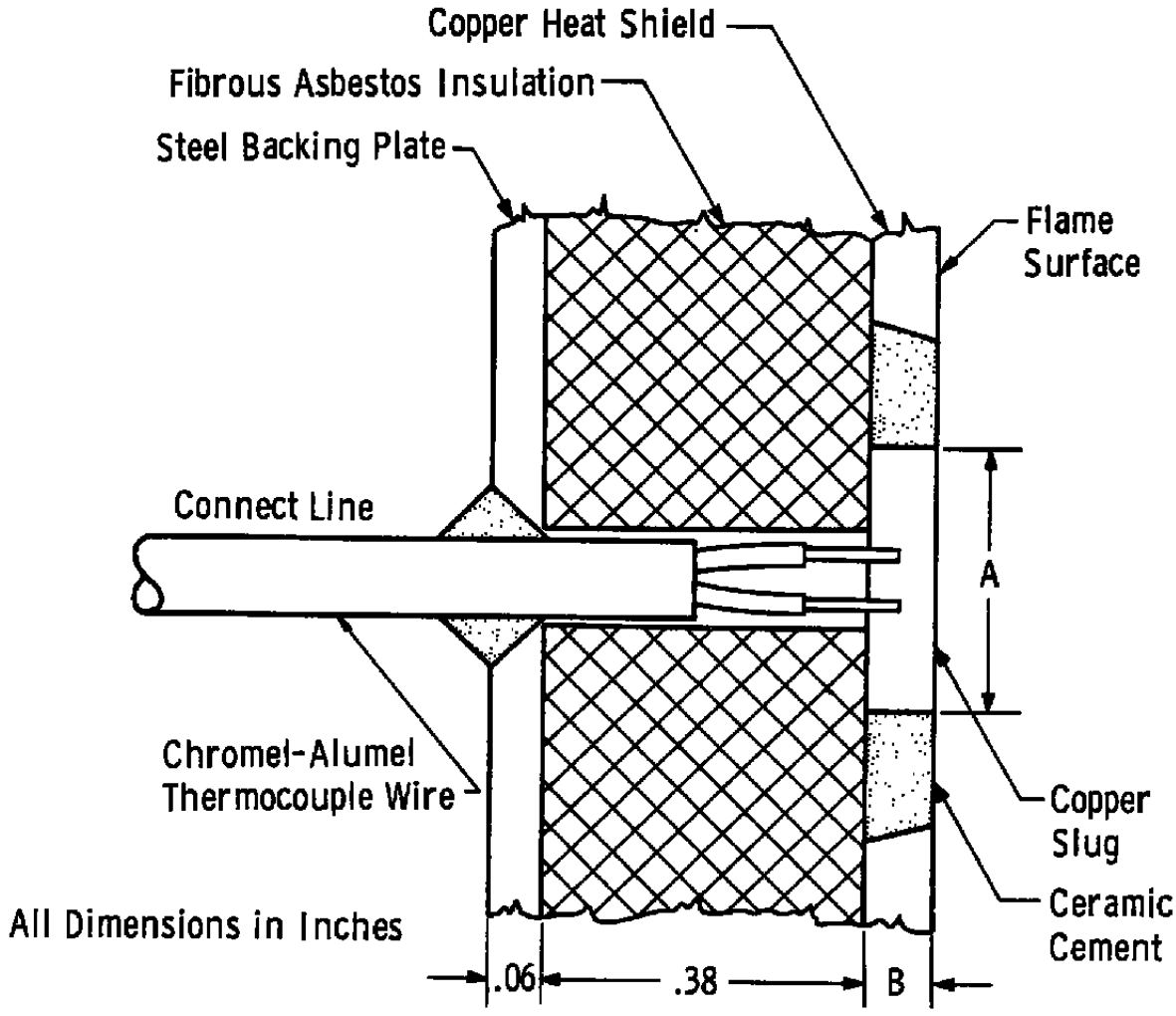

Calorimeter Slug Dimensions

	Heat Shield	Flame Shield
A (diam)	0.4375	0.250
B	0.065	0.104
Nominal Weight of Slugs, gm	1.397	1.290

Fig. 8 Details of Heat and Flame Shield Calorimeters

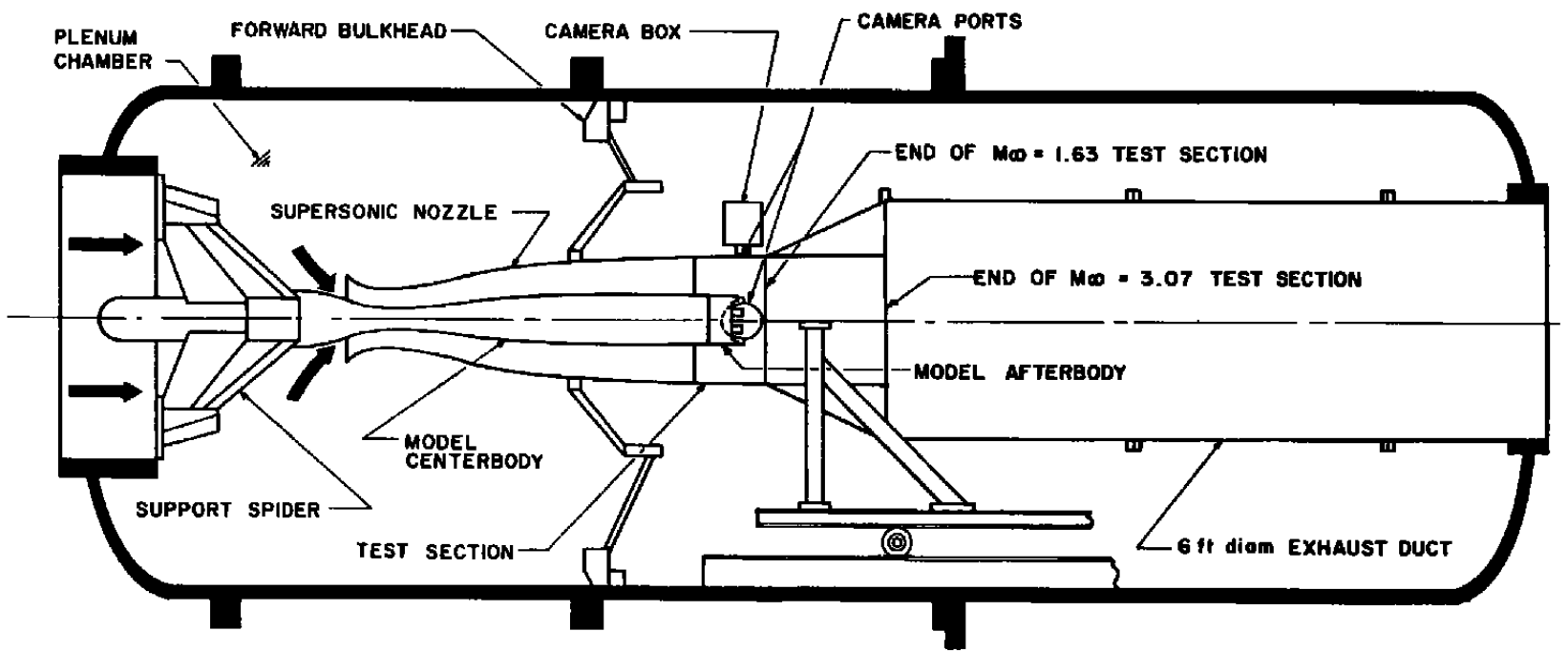

Fig. 9 Schematic of Model Installation in Rocket Altitude Cell T-1

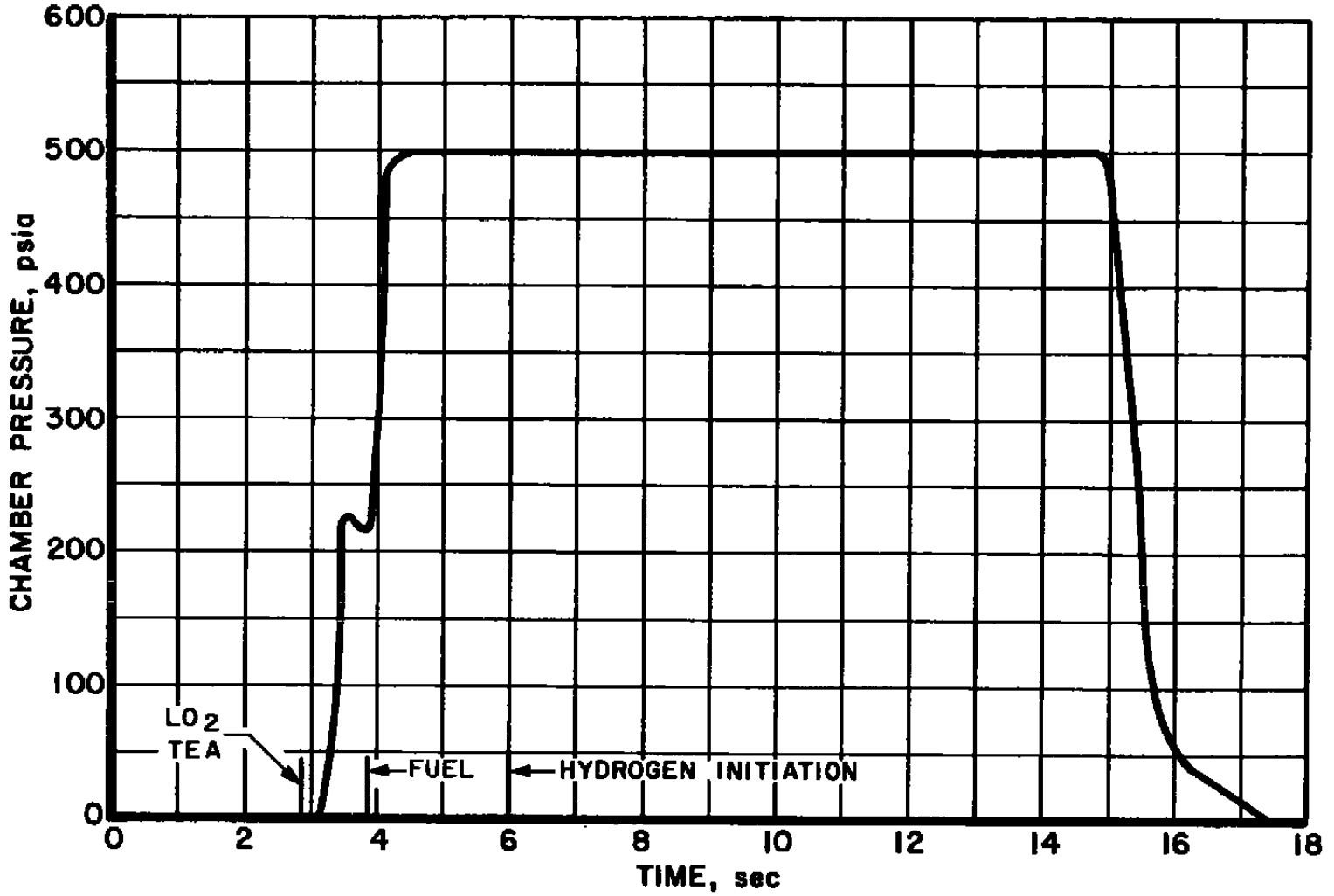

Fig. 10 Typical Engine Chamber Pressure Time History

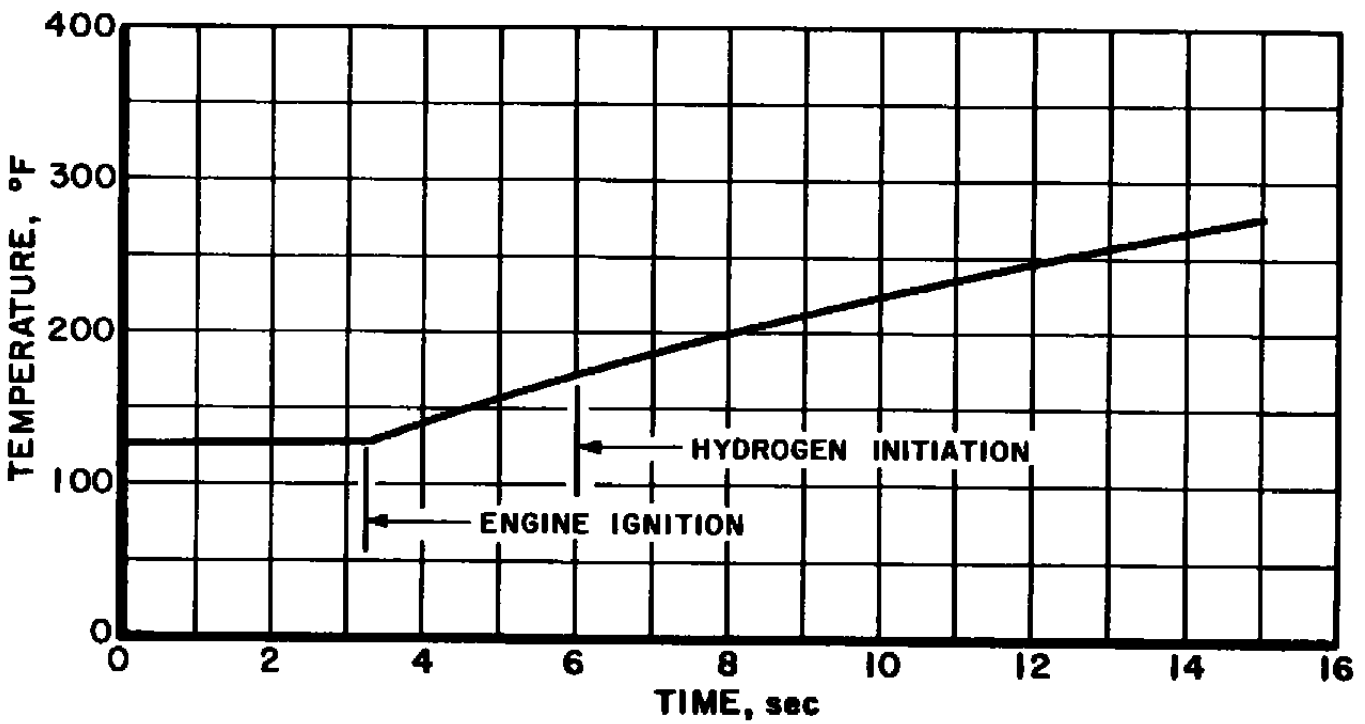

Fig. 11 Temperature Variation with Time for Base Heat Shield Calorimeters (Typical)

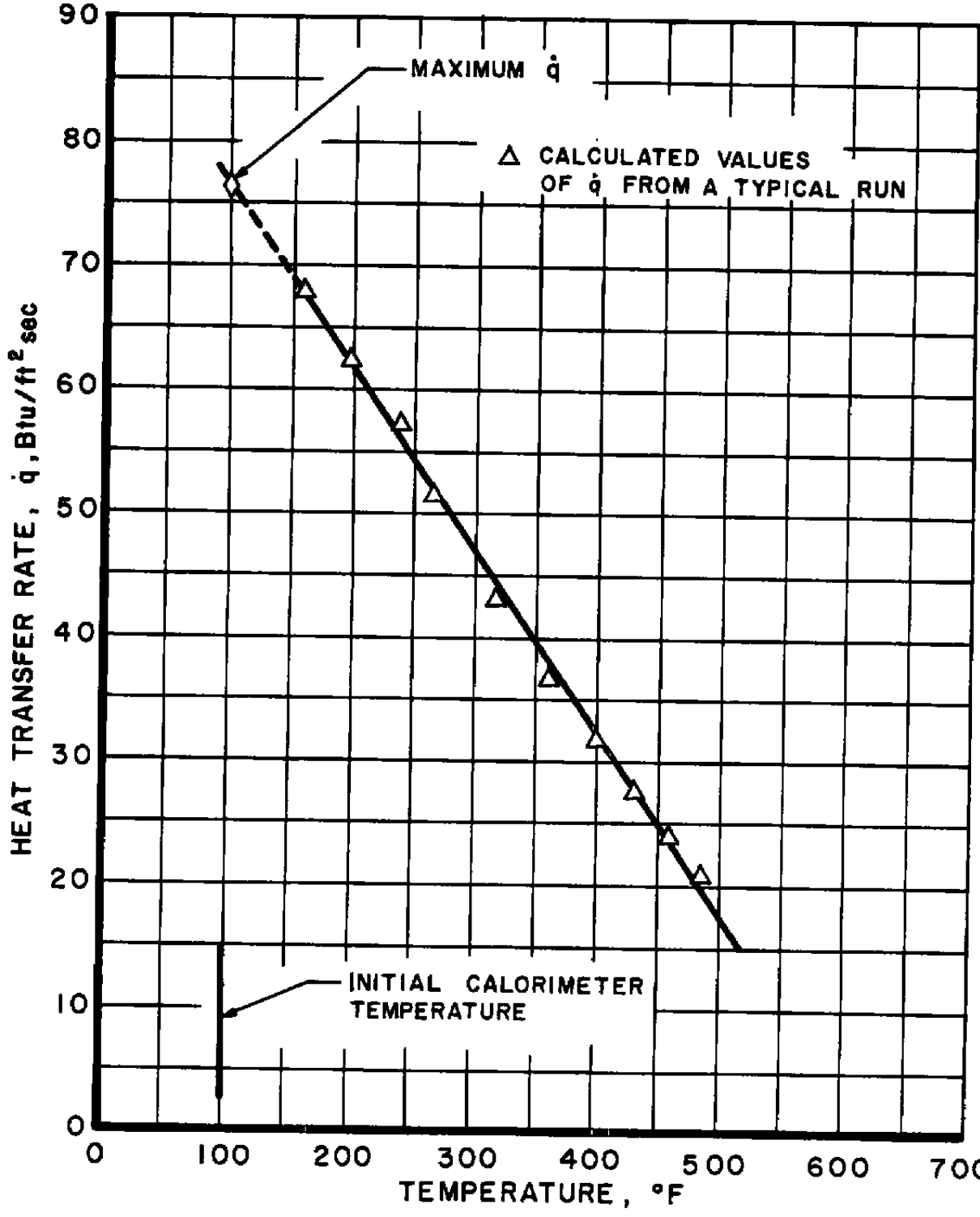

Fig. 12 Heat Transfer Rate Variation with Temperature for a Flame Shield Calorimeter (Typical)

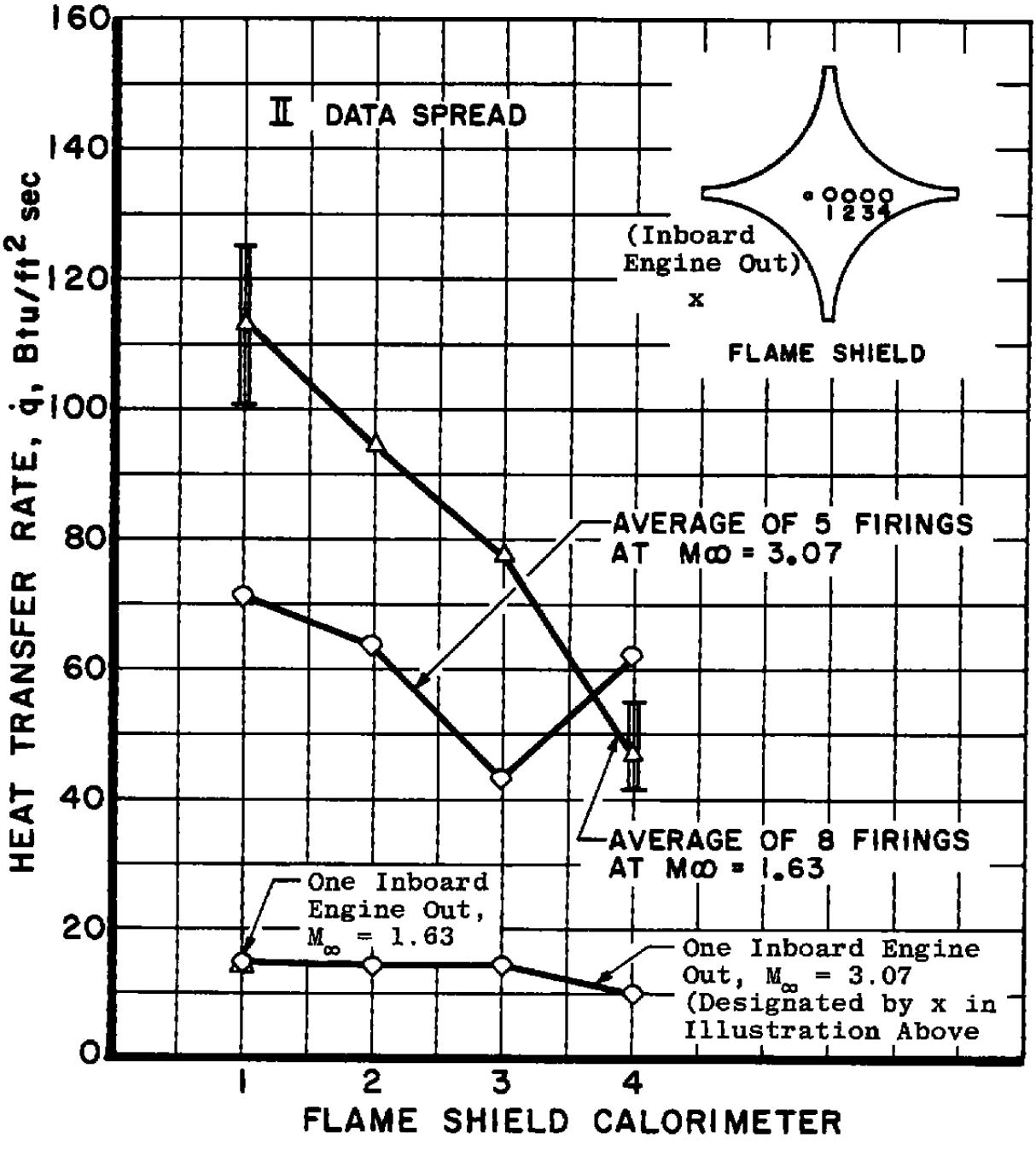

Fig. 13 Heat Transfer Variation with Flame Shield Calorimeter Location

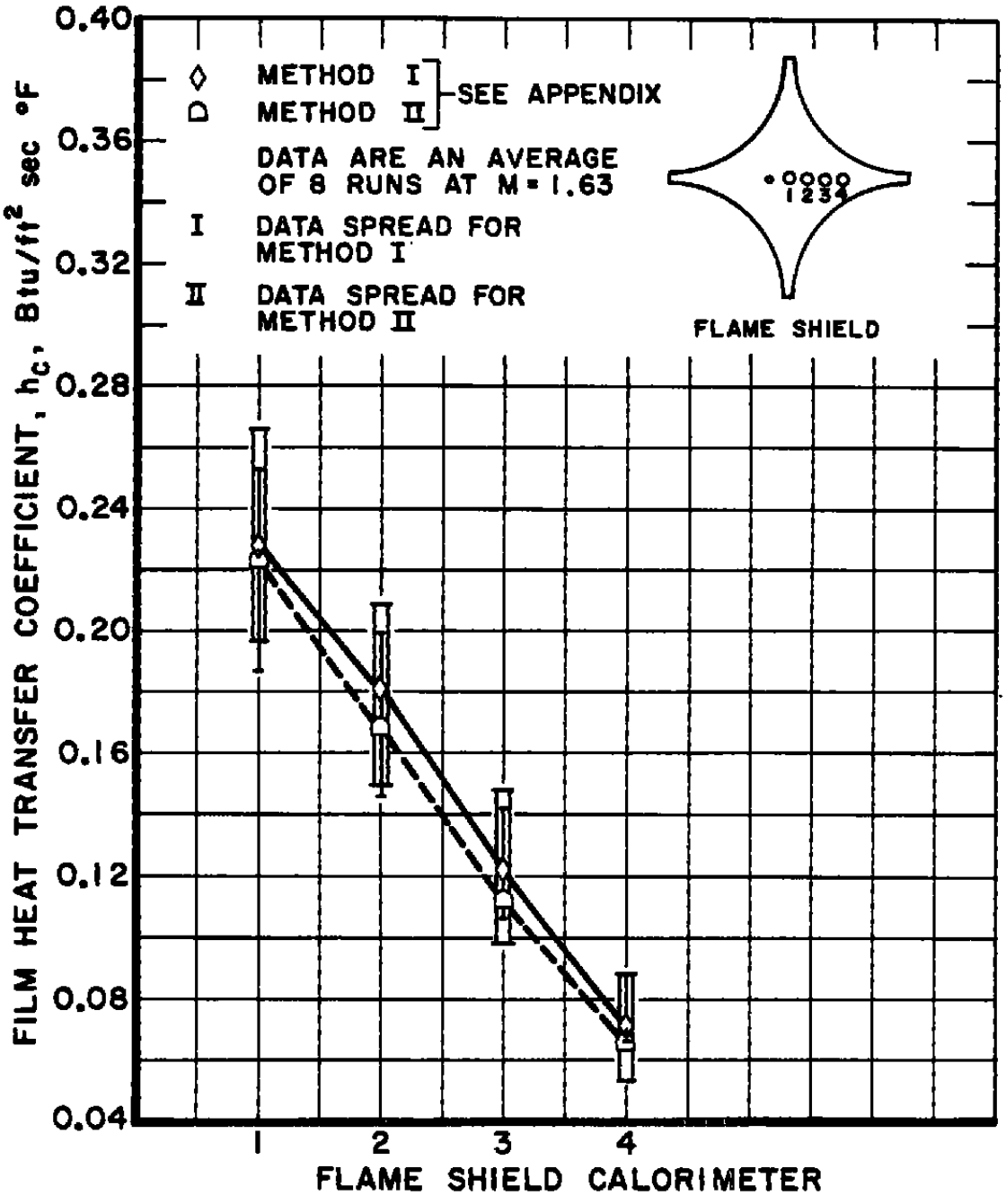

a. Film Coefficient at M ≈ 1.63

Fig. 14 Film Heat Transfer Coefficient Variation with Flame Shield Calorimeter Location

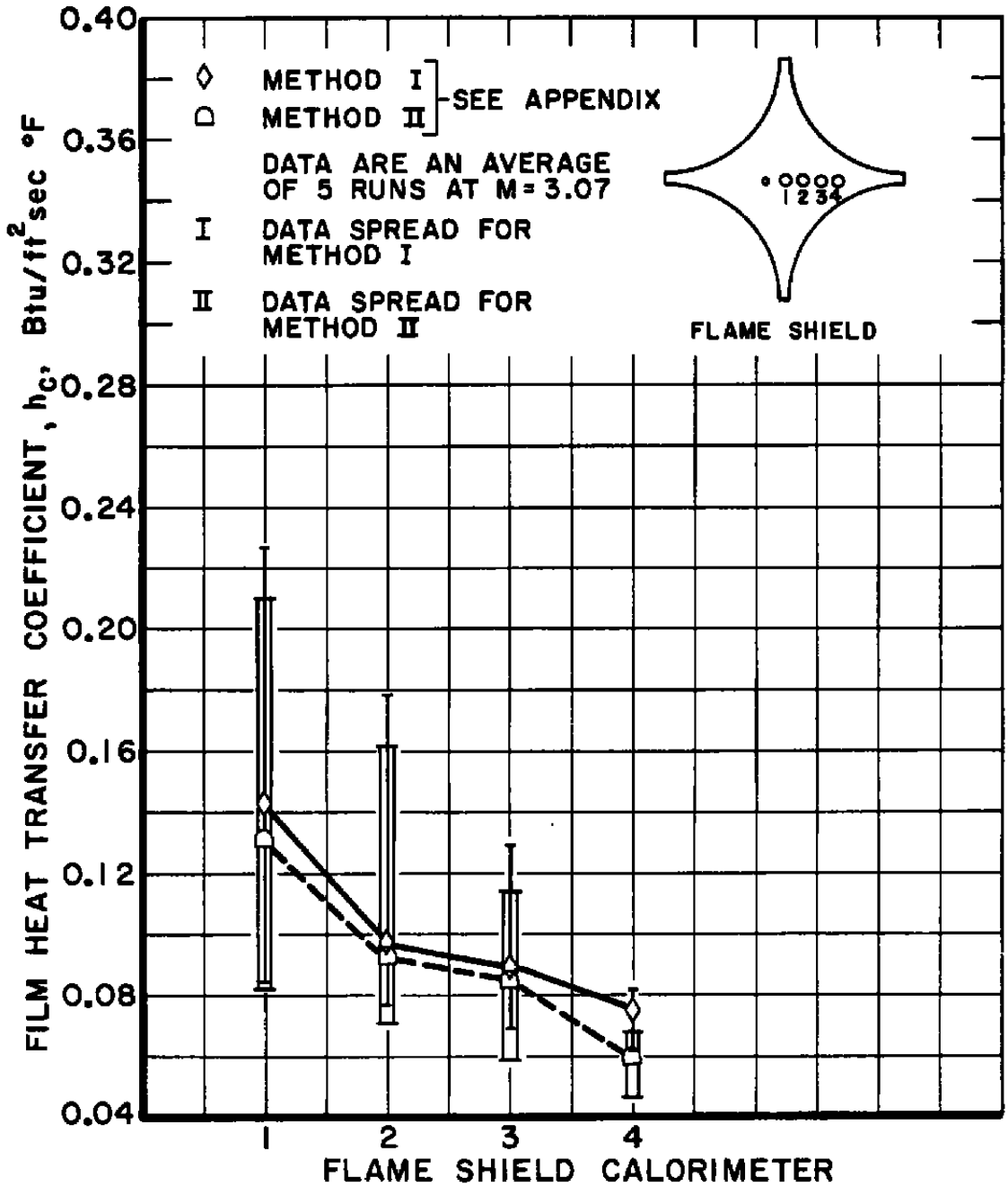

b. Film Coefficient at M = 3.07

Fig. 14 Concluded

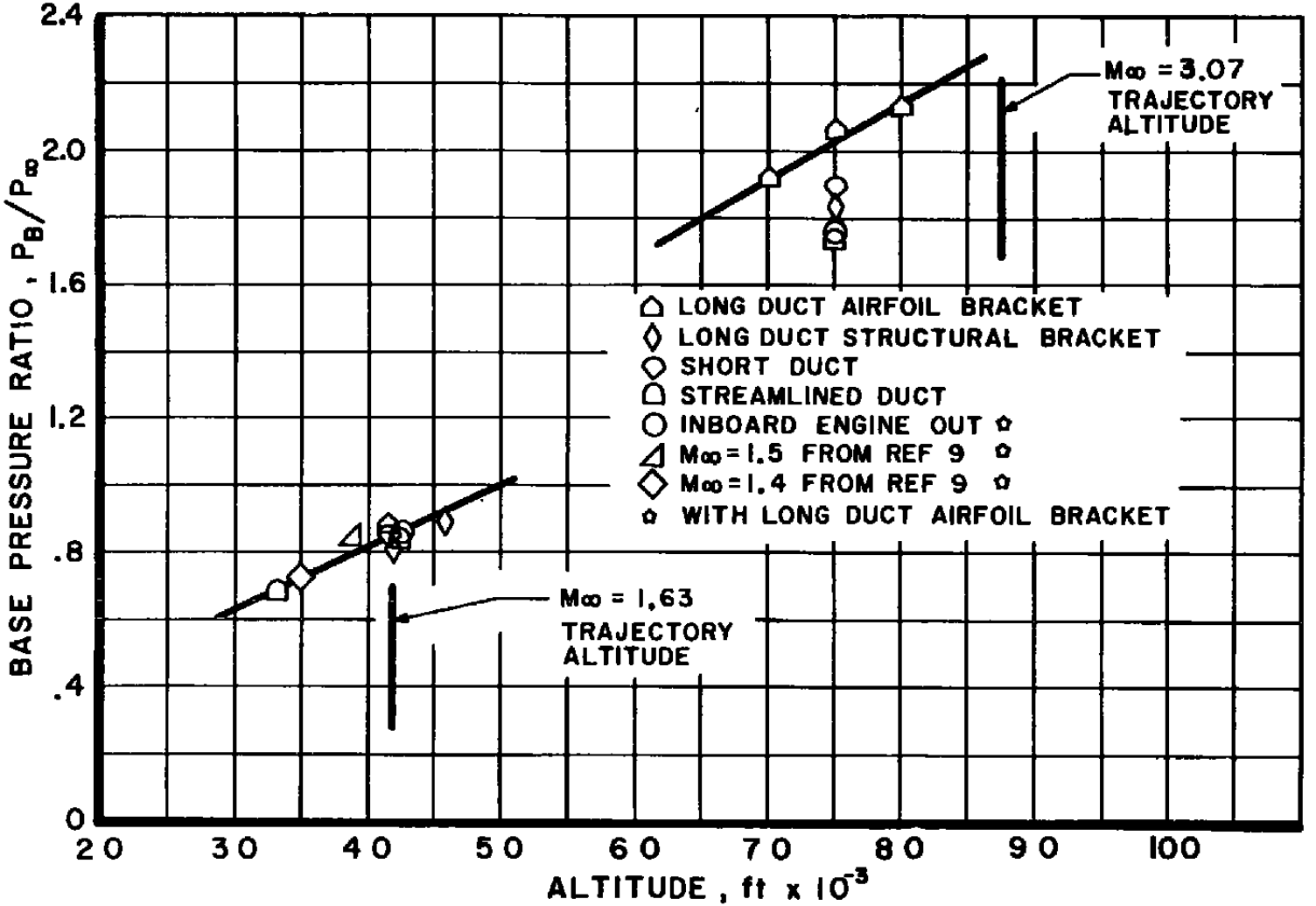

Fig. 15 Variation of Base Pressure Ratio with Altitude

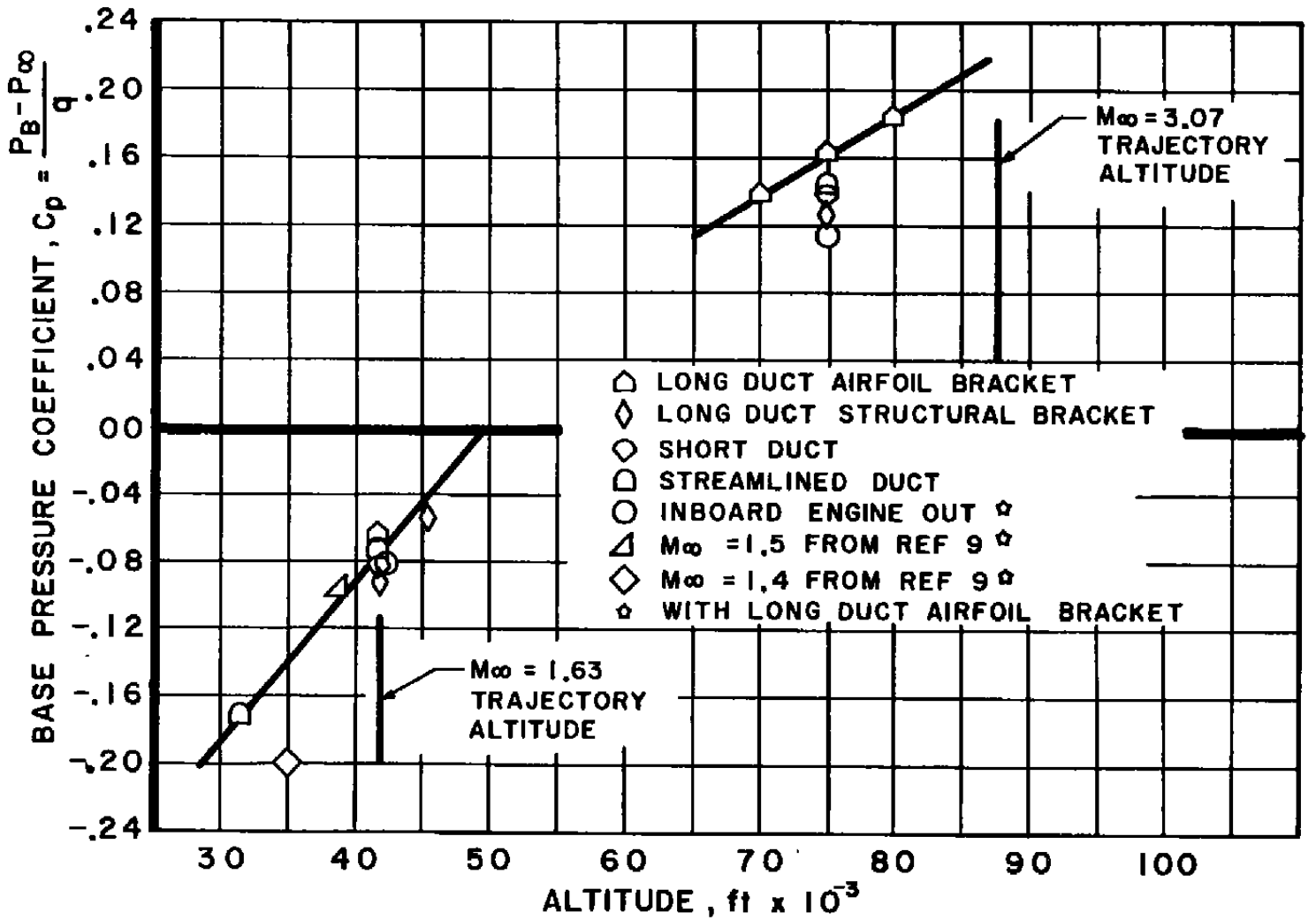

Fig. 16 Variation of Base Pressure Coefficient with Altitude

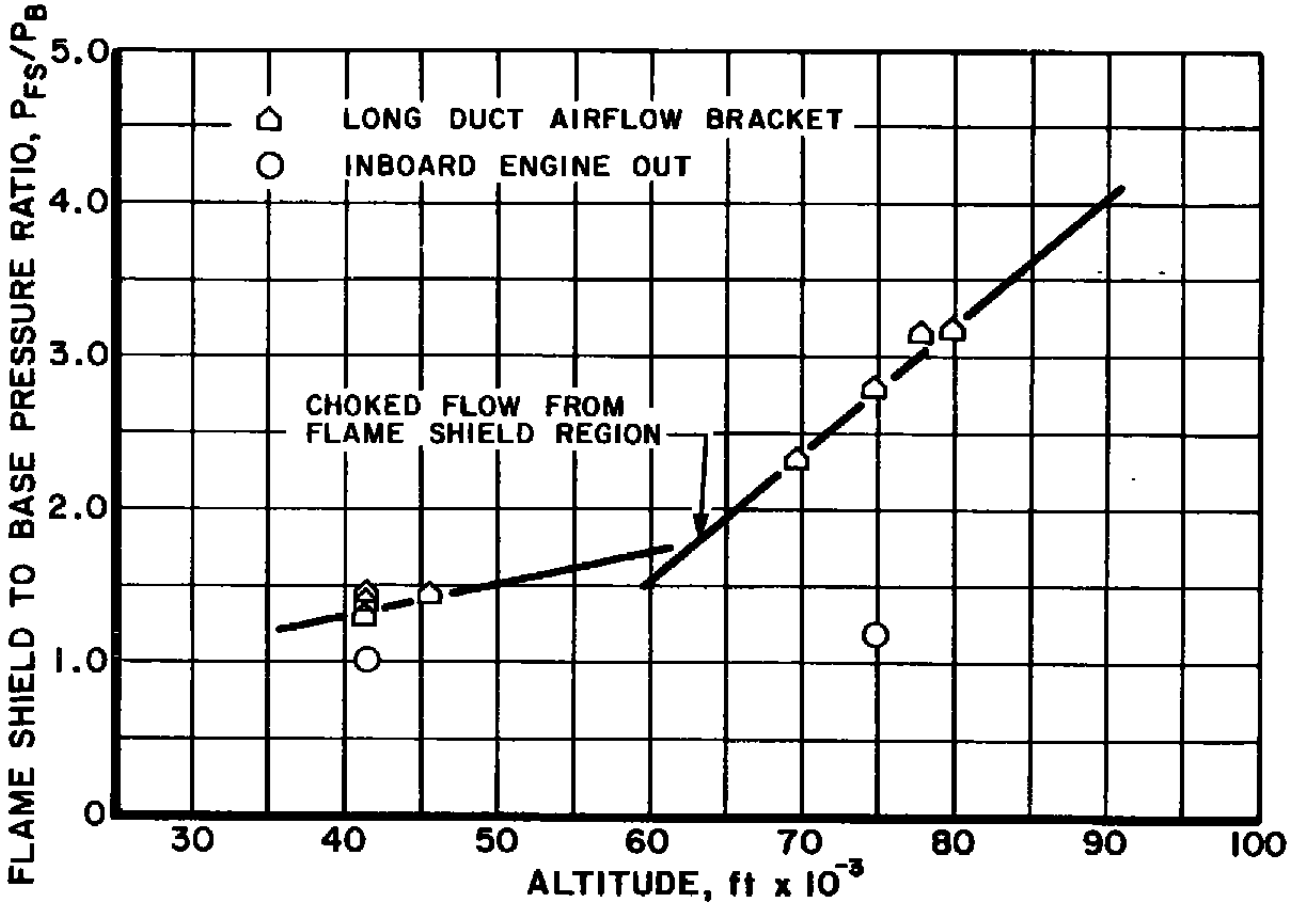

Fig. 17 Variation of Flame Shield Pressure Ratio with Altitude